Universidade de Aveiro
Departamento de
Electrónica, Telecomunicações e Informática
2016

Diogo
Fonte
da Silva

Validação e Instrumentação de Sensores SAW para Medição de Binário e Temperatura

SAW Sensor Validation and Instrumentation for Torque and Temperature Measurement

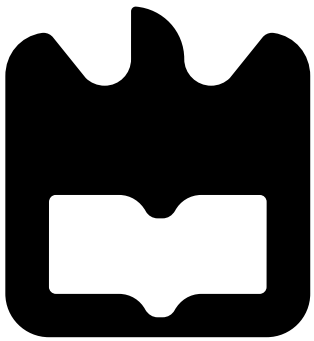

Diogo
Fonte
da Silva

Validação e Instrumentação de Sensores SAW para Medição de Binário e Temperatura

SAW Sensor Validation and Instrumentation for Torque and Temperature Measurement

Dissertação apresentada à Universidade de Aveiro para cumprimento dos requisitos necessários à obtenção do grau de Mestre em Engenharia Eletrónica e Telecomunicações, realizada sob a orientação científica do Professor Doutor Luís Nero Alves do Departamento de Eletrónica, Telecomunicações e Informática da Universidade de Aveiro e da Doutora Joana Catarina Mendes do Instituto de Telecomunicações da Universidade de Aveiro.

O júri / the jury

Presidente / President

Professor Doutor Paulo Bacelar Reis Pedreiras
Professor Auxiliar, Universidade de Aveiro

Vogais / Examiners committee

Doutora Joana Catarina Martins Mendes
Bolseira de Pós-Doutoramento, Instituto de Telecomunicações (Co- Orientador)

Doutor Edoardo Detoma
Físico Consultor em Engenharia de Sistemas Rf, L J T & Associates

Agradecimentos

É com grande orgulho que aproveito esta oportunidade para em primeiro lugar agradecer aos meus pais por graças ao seu esforço e dedicação, me terem dado a oportunidade de ter educação de grande qualidade, durante o meu crescimento quer a nível pessoal, quer a nível de formação académica. Um especial obrigado também a todas as outras pessoas, nomeadamente a minha namorada pelo seu incansável apoio e incentivo neste trajeto e ainda parentes, amigos e antigos professores, que de alguma forma contibuiram com apoio ou ensinamentos, nesse mesmo crescimento.

Quero também agradecer ao professor Luís Nero Alves do Departamento de Eletrónica, Telecomunicações e Informática da Universidade de Aveiro e professora Joana Catarina Mendes do Instituto de Telecomunicações da Universidade de Aveiro pela sua orientação. Os seus conselhos, críticas e ensino foram vitais na realização deste trabalho. Deixo ainda ao Doutor Edoardo Detoma, arguente da prova de avaliação desta mesma dissertação, uma nota de apreço por ter fomentado uma discussão que contribuiu para um melhor entendimento e aprofundamento de algumas das conclusões a retirar deste trabalho. Um estimado agradecimento ao professor António Bastos e ao Engenheiro Ricardo Beja do Departamento de Engenharia Mecânica da Universidade de Aveiro pelo seu contributo e transmissão do seu conhecimento, a nível da compreensão científica do trabalho de engenharia mecânica a realizar e da própria montagem do equipamento mecânico, indispensáveis à realização deste trabalho. Por último, um grande obrigado aos meus colegas Francisco Felício, João Pereira, António Ramalho e Bernardo Fernandes do curso de Engenharia Mecânica da Universidade de Aveiro, pelo seu muito importante contributo no projeto e montagem dos set- ups de medição.

Resumo

O trabalho aqui apresentado está inserido no âmbito do projeto RTMGear, que visa a instrumentação e medição de grandezas físicas tais como binário e temperatura, diretamente a partir dos componentes rotativos da caixa de transmissão de testes, com a finalidade de validar a tecnologia usada para aplicação na indústria aeroespacial.

A tecnologia estudada para realizar a monitorização em tempo real de tais grandezas são sensores SAW (sensores de onda acústica superficial) que se tratam de componentes microeletromecânicos (MEMS), com capacidade de medição em ambientes com condições difíceis como o que está a ser estudado.

Com o objetivo de proceder ao estudo referido, dois set- ups mecânicos foram construídos e um conjunto de testes para estudar o comportamento dos sensores em tais condições foi efetuado:

O primeiro, um set- up estático foi concebido para proceder à calibração dos sensores de binário para medição desta mesma grandeza, obtendo a curva de variação da sua resposta em função da gama de binário aplicada com recurso a uma máquina de testes universal. Foram ainda efetuados dois testes (um por tipo de sensor) com o intuito de obter as curvas de dependência dos sensores relativamente à temperatura.

O segundo, um set- up dinâmico com capacidade de atingir rotação até próximo das 2500 rpm e com capacidade de proceder ao aquecimento da área de aplicação dos sensores até temperaturas superiores às compreendidas na sua gama de funcionamento. Neste Set- up testes para avaliar o efeito da aplicação de velocidade de rotação e temperatura no erro de medição e testes finais para apurar o binário medido com compensação do efeito da temperatura, após calibração prévia, foram efetuados.

Os resultados obtidos com os procedimentos experimentais descritos permitiram retirar numerosas conclusões sobre o trabalho realizado mas são insuficientes para validar a aplicação da tecnologia. Para tal, seriam necessários testes de medição de binário numa gama superior, com compensação de temperatura fossem realizados para valores de velocidade de rotação e temperatura significativamente superiores ao caso apresentado em que valores de binário foram efetivamente extraídos da realização experiemtal

Abstract

The work here presented is inserted in the framework of the RTMGear Project, that has the objective of measuring several physical parameters, such as torque and temperature, directly within the rotating parts present in a power reduction gearbox. The urge of this study comes from the aircraft industry demand for systems able to perform real-time monitoring of torque in the most critical components operating inside a gearbox. However, the existing sensing technologies have limitations in terms of accuracy. There are also considerable difficulties to its implementation such as space constraints and very harsh conditions which make inappropriate the use of cables and electronic devices inside the gearbox.

For this effect, sensing devices based in SAW(Surface Acoustic Waves) technology were used. This devices are microelectromechanic (MEMS) systems whose characteristics are appropriate to the harsh conditions at hand.

In order to proceed with the study two mechanical set- ups have been fabricated, to support the sensors evaluation tests. The first consisted in a static set- up designed to proceed to the calibration of the strain sensors for torque measurement. The second was a dynamic set- up designed to reach rotation speed as high as $\approx$2500 rpm and with the capability of heating the sensors application area above its operating range. This set- up accommodated tests to evaluate the effect of speed and temperature in the uncertainty of the measurements and finally, an experiment to perform torque measurement with temperature compensation was made.

Tests to evaluate the curve dependence of the SAW sensors wrt temperature and the communication link established by two special antennas designated as RF rotary Couplers, used to establish wireless connection in rotative set-ups were also realized.

The results obtained allowed the achievement of several conclusion regarding the work done and future improvements, given that a complete study on the sensors behaviour with respect to the physical quantities being analysed was made and conclusions about the effect of speed and temperature in the measurements are obtained. However, in order to obtain validation of the technology for gearbox instrumentation, actual torque measurements in a broader range (0 to 250 Nm) with compensation of temperature and vibration, under broader ranges of speed (up to 3000 rpm) and temperature (between -25 °C up to 85° C or more) would have to be accomplished.

Contents

List of Figures

List of Tables

List of Acronyms

SAW - Surface Acoustic Wave
UHF - Ultra High Frequency
RF - Radio Frequency
DC - Direct Current
MHz - Megahertz
GHz - Gigahertz
RTM - Real Time Monitoring
IDT - Interdigital Transducer
SNR - Signal to Noise Ratio
IF - Intermediate Frequency
RFID - Radio Frequency Identification
RLC - Resistor-Inductor-Capacitor
BvD - Butterworth Van Dyke
Q - Quality Factor
BW - Bandwidth
SAWR - Surface Acoustic Wave Resonator (single)
SAWDR - Double Surface Acoustic Wave Resonator
TCF - Temperature Coefficient
RADAR - Radio Detection And Ranging
VNA - Vector Network
FDS - Frequency Domain Sampling
DDS - Direct Digital Synthesis
DAC - Digital-to-Analog Converter
ADC - Analog-to-Digital Converter
ISM - Industrial, Scientific and Medic (Radio Band)
PA - Power Amplifier
LNA - Low Noise Amplifier
LO - Local Oscillator
SNR - Signal-to-Noise Ratio
AWGN - Additive White Gaussian Noise
NF - Noise Factor

FFT - Fast Fourier Transform
DFT - Discrete Fourier Transform
IDFT - Inverse Discrete Fourier Transform
BHN - Blackmann- Harris- Nuttall
wrt - with respect to
CAD - Computer Assisted Design
PCB - Printed Circuit Board
GUI - Guide User Interface
GPa - Giga Pascal

Chapter 1

INTRODUCTION

Throughout the years the real-time monitoring of aeronautical mechanical systems has gained crescent interest by the aircraft industry. Efficient monitoring can both provide enhanced safety and maintenance cost reduction. These measurements can extract direct information about the most critical components operating inside a gearbox, however there are some serious difficulties to its realisation.
For starters, there are significant constraints in terms of space. Electronic systems inside a gearbox are expected to face extremely harsh conditions due to existing centrifugal forces, oil flow in the rotative components and high operating temperatures. At last, acquiring data from rotating parts might be challenging in terms of power transmission and communication between the sensing elements and the electronic modules. The usage of SAW sensors might ensure solutions for the issues presented.
Application of SAW devices to non-contact torque measurement was first suggested and patented in [1]. With the advances of microelectronics in the early 90's and the maturation of SAW technology, its application as passive wireless sensors has gained interest from many industries, since compact and inexpensive design of readers became feasible, and the low cost in SAW devices production and reproducibility was achieved, for UHF [2].
SAW piezoelectric passive sensors enable wireless sensing, via RF at considerable distances, at almost no energy consumption, since they do not require DC power from batteries and work as back- scatters with the frequency response dependant on the physical quantity to be measured.
Also, it's very small dimensions, high lifetime without the need of maintenance, resistance to harsh conditions, reliability and the possibility of large manufacturing of volumes of all sorts of physical sensors, such as temperature, pressure, load, acceleration and torque sensors, make them particularly well suited for aerospace and automotive applications such as gearbox instrumentation, where wired and high dimension electronics, would be problematic. Besides this, SAW devices possess high Q factors (> 10000, typically), allowing high resolution wireless measurements in comparison with other competing technologies. [2–6]
SAW sensors are also insensitive to stray magnetic fields and tolerant to variation of distance

between the reader and the sensor antenna, unlike magneto- elastic and Hall effect sensors, two of this competing technologies, and have very high sensitivity to strain, allowing them to be used in standard or slightly modified automotive parts [2].
In fact, there is a clear demand for sensing torque, since adequate condition monitoring would be critical for predictive and corrective maintenance, that would notably reduce costs in industries such as renewable energy collection from wind turbines, where 80% of it's maintenance cost, it's due to unexpected failures of rotating components [7].
In aircraft industry, it is estimated that $\approx 40\%$ of the maintenance costs is due to repair and direct labour, at engine shop visit, and even the other $\approx 60\%$, due to material replacement cost, could be significantly decreased, if proper engine condition monitoring would be done, and engine shop visits would be scheduled when necessary, in conformity with the results obtained [8].

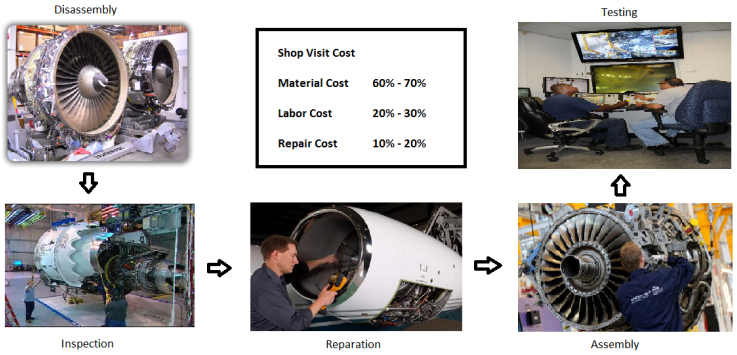

Figure 1.1: Engine shop visit cost statistics, according to [8]

There are already some commercial solutions available for fault detection across aeronautical mechanical systems. A great deal of the the monitoring applications are realized recurring to data signals acquired from non- rotating parts, like from oil quality analysis, proximity sensors, acceleration sensors, sound emission, temperature and pressure.
Relatively to oil quality analysis, it is a mature technology in which fault detection is made by detection of the metallic particles in the oil flow, either through detection of induction variation caused by moving metal particles in the oil flow or through the use of magnetic chips that collect metallic chips and check their amount size. Proximity sensors have a great role in structural health monitoring, by providing information about the wearing level of the mechanical parts, by measuring misalignments in the rotating axes, or by directly measuring accurate height of the gear teeth. This methods are matured technologies, however since these are indirect measurement that don't necessarily give information about the forces applied in the rotative apparatus and the material deformations, can't offer the accuracy of the SAW technologies [9–11].
Measuring directly in the system rotating parts allow the measuring of structural information directly from the most critical pieces, and is currently a topic under maturation. The commercially available solutions consist on Metal foil strain gages, which are properly attached

with a suitable adhesive to the surface under test, measuring its elongation. Fiber-optic strain sensors, which work by analysis of the internal reflections caused by changes in the cavity refractive indices. This sensors have low temperature sensitivity but it could present difficult to support its electronics inside a gearbox. New approaches to strain gages have been developed using thin-film technologies with photolithography and laser processing. [12]
Magnetostrictive sensors could also provide direct measurements in the rotative components. They work by detection of magnetic fields caused by the material deformation and could also be a valid solution but are still under development for aerospace applications [13]. Finally, RF powered LC sensors are passive, contactless and are a solution also employed for measurements of temperature but have lower quality factor Q than saw sensors [14].

1.1 Motivation and Framework

This dissertation was developed under the framework of Project RTMGear, that aims at the instrumentation of an airplane gearbox. The purpose of the present document is to describe the experimental set-ups and methodologies that have been used, in order to validate the usage of SAW sensors to perform real- time measurements of temperature and strain inside a power reduction gearbox and consequently, to determine if the acquired commercial SAW sensing equipment presents itself as a valid solution.

1.2 Thesis Objectives

Given the context previously presented, we can define the main goals of this work as the validation of SAW technology for gearbox instrumentation, considering the following:

1) Characterization of both the temperature and strain sensors by obtaining the calibration curves with which the measurements will be realized.

2) Evaluation of the the effect of speed and temperature in the uncertainty of the measurements of both the temperature and the strain sensors under their operating range.

3) Performing accurate measurements using commercially available devices. For this approach, a read-out unit from SENSeOR, operating in the 433 MHz band employing frequency domain sampling, supporting interrogation of multiple sensors at the same time, aiming at the measurement of temperature and torque, will be used.

4) Achievement of conclusions regarding to which details, in a future work, a technician should have attention during the manipulation of the sensors and about future improvements to the experiment.

1.3 Thesis Structure

This document structure comprehends four chapters, whose contents can be described as follows:

2) Insight into the current state of the technologies, techniques and methodologies, employed in the work done and presented in this document, referring what is already been done and by whom.

3) A complete description of the practical techniques and set-ups employed to validate and characterize the commercial solutions employed in this work, the major practical problems and concerns found, during the process.

4) Presentation of the results obtained performing the SAW device measurement procedures using commercial available devices. Analysis of the obtained data.

5) The final chapter, describing the main conclusions taken from the realization of this work: were the initial objectives achieved? If not, why were they not achieved and what would need to be changed to achieve them. Presentation of proposals for improvements and future work to follow.

Chapter 2

SAW SENSORS, INTERROGATION AND SIGNAL PROCESSING METHODOLOGIES

Before advancing to the practical realization of the activities proposed for this work, it is important to do a careful survey on the SAW technology to be used. The interrogation methodologies used to acquire the information sensed by the device and the general architecture of the read-out units that make the interrogation. Gathering information about what is available to the public, shall allow a better comprehension on the essential issues and points to be improved in the technology.
The knowledge acquired will be exposed in this chapter, giving focus to the details that will be used in this work, and to the reasons of some of the choices taken to achieve the defined objectives. This chapter is structured as follows:
First, a brief introduction on the SAW technology upon which the sensors to be used are based. Next a presentation of the general architecture of the Read-Out units used is given and a survey on interrogation techniques used by such devices as well as its limitations is made.

2.1 Brief introduction to SAW sensors

A Surface Acoustic Wave (SAW) is a type of acoustic wave travelling in a solid material surface, that presents elastic properties. The particles motion amplitude due to SAW, suffers exponential attenuation with material's depth, and usually can be considered negligible for depths over one wavelength.
They were first explained by Lord Rayleigh, in his classic paper of 1885 *"On Waves Propagated along the Plane Surface of an Elastic Solid"*, and divided into two types of waves:
- Love waves, with particle motion in a horizontal line, perpendicular to the direction of propagation.

- Rayleigh waves, with a longitudinal and a vertical shear component, suffering little attenuation as they progress on the surface, generating elliptical solid particles movement along the path, as illustrated in the figure 2.1 [6].

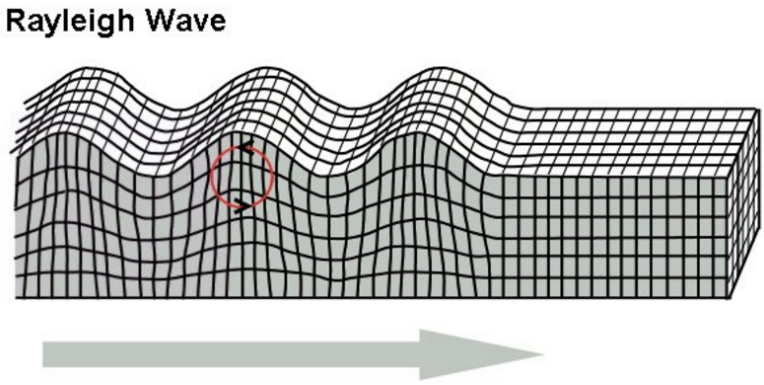

Figure 2.1: Rayleigh wave model of propagation [15]

The SAW coupling with it's propagation medium, strongly affects the amplitude and velocity of the wave. In the case of the propagation being in a piezoelectric substrate, an electric signal can be transduced into a mechanical signal, by generation of surface acoustic waves. The coupling between the received electric signal and the medium is extremely sensitive to variation in the material's conditions, enabling the sensing of mechanical properties using SAW-based devices as electronic components. The surface waves velocity of propagation is dependent to the piezoelectricity, elasticity and dielectric characteristics of the material, and the propagation velocity variation with these properties, is in its turn, dependent on the sensitivity of these same properties to temperature. These properties for a few different materials and substrate geometries can been seen in the table 2.1.

Table 2.1: Physical constants dependence to material and orientation choice, from [6,16–18]

Material Orientation (1)			Vph	K	TCD	Attenuation (db/us)	
Substrate	Cut	Propagation	(m/s)	(%)	(ppm/°C)	433 MHz	2.45 GHz
Quartz	ST	X	3158	0.1	0	0.75	18.6
(SiO_2)	37° rot Y	37° rot Y	5094	0.1	0	(2)	(2)
Lithium niobate	Y	Z	3488	4.1	94	0.25	5.8
($LiNbO_3$)	41° rot Y	X	4750	15.8	69	(2)	(2)
	128° rot Y	X	3980	5.5	75	0.27	5.2
Lithium tantalate	36° rot Y	X	4220	6.6	30	1.35	20.9
($LiTaO_3$)	X	112° rot Y	3301	0.88	18	-	-

(1) Cut and material orientation in relation to the surface's normal.

(2) Value depends on the metallization ratio of the IDTs.

For high temperature applications materials such as berlinite (AlPO4), lithiumtetraborate ($Li_2B_4O_7$), langasit ($La_3Ga_5SiO_14$) and galliumorthophosphate($GaPO_4$), can be used up to 1000 ^oC [19].
The transduction from electric signal into a mechanical surface wave, comes from the direct coupling between the signal source and the piezoelectric substrate, realized by two interdigitized shaped arrays of metallic electrodes, called IDTs (interdigital transducers), illustrated in figure 2.2, deposited on the surface of the piezoelectric substrate [6,19,20].
SAW technology started being implemented at first in electronics and instrumentation due to the need for developments in radar systems. Filters based in transmission lines and passive L-C components for pulse compression and SNR optimization were too volumous and of difficult practical execution. SAW devices, with much smaller velocity of propagation were the natural choice for the realization of the same filters in a much more feasible and compact way [6].
The first practical realization of such ideas was made in 1965 in the classical article by R. White and F. Voltmer, *" Direct Piezoelectric Coupling to Surface Elastic Waves "* [21]. The uniform configuration for IDTs, proposed at the referred article had a distance between two IDT fingers and it's thickness, both equal to $d = \frac{\lambda}{4}$.

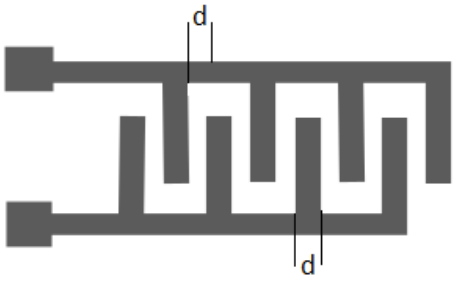

Figure 2.2: SAW interdigitated transducer [21]

Then, in 1969 the Tancrell group published an article named *"Dispersive delay lines using ultrasonic surface waves"*, with the first reliable delay line composed by two reciprocal IDTs (both can be used as in and out ports), on each extremity. In fact, a SAW-based delay line is the simplest wideband sensor as illustrated in figure 2.3, characterized by the propagation delay dependence on the physical quantity being measured [6,22].
The usage of IDT's as reflectors allowed the appearance of several commercially available devices, such as resonators, RF and IF filters, actuators, duplexers and RFID Labels, for example. In the case of RFID labels the identification can be made by the pattern coded through the device's reflectors position [4,6,19].

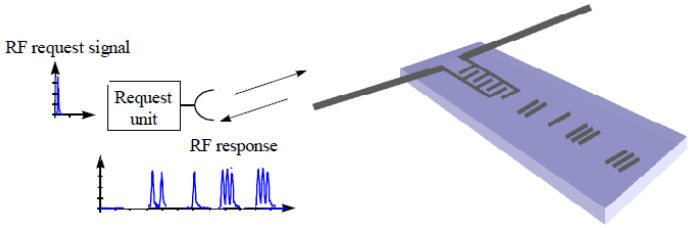

Figure 2.3: SAW-based reflector device, functioning model [4]

Another SAW-based device is the Impedance Sensor (figure 2.4), obtained through the use of IDTs as reflectors with appropriate load impedances. The reflection coefficient varies with the load impedance, dependent on the physical quantity being investigated. The advantage in the usage of this kind of device is the separation between the RF transponder and the actual sensor, being the measurement obtained indirectly. This solution also allows chip packaging and better insulation from deterioration [4, 5, 19].

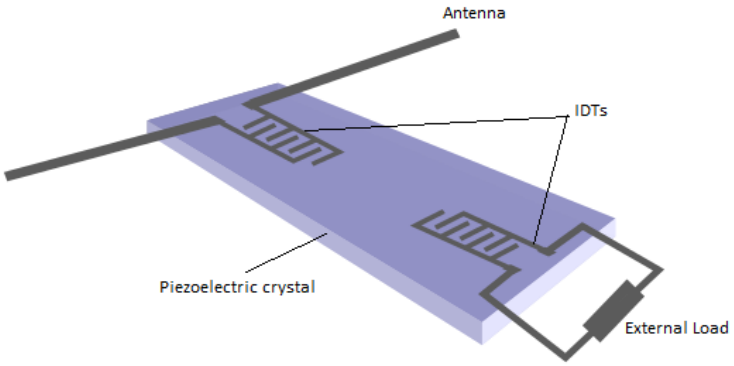

Figure 2.4: Impedance SAW-based sensor diagram [4, 5]

2.2 SAW Resonators

From the devices previously mentioned, SAW resonators are particularly well suited for sensing applications, and so, are the ones used during this work. These devices are significantly narrowband, which results in sensitivity gain, better resolution in the measurement and better efficiency in terms of energy.

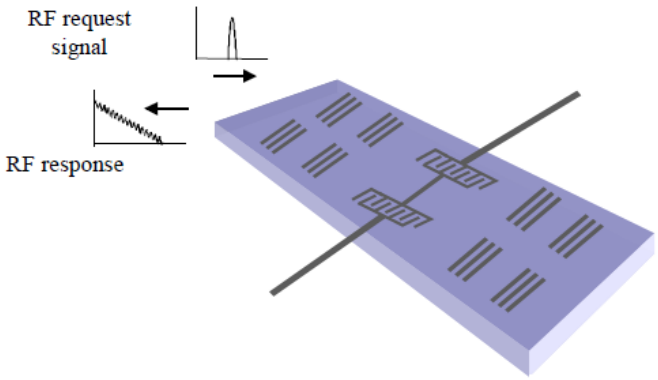

Figure 2.5: SAW resonator sensor example [4]

The operating resonant frequency is obtained from a compromise between the materials chosen, from which depends the velocity of propagation of the acoustic wave and the dimensions of the IDT.
Succinctly, SAWRs operating principle is the following: once the electromagnetic signal request signal is captured by the antenna, it is transduced into a mechanical acoustic wave in the IDT. The mechanical wave travels with elliptical trajectory in the surface of the sensor piezoelectric substrate. The velocity of propagation depends on the material conditions. The SAW is reflected and transduced back into a response electromagnetic wave. The time variation in the response release is translated into a change in the device resonant frequency, from which the physical quantity is sensed using an adequate read-out unit [19, 23]. This principle is illustrated in image 2.6:

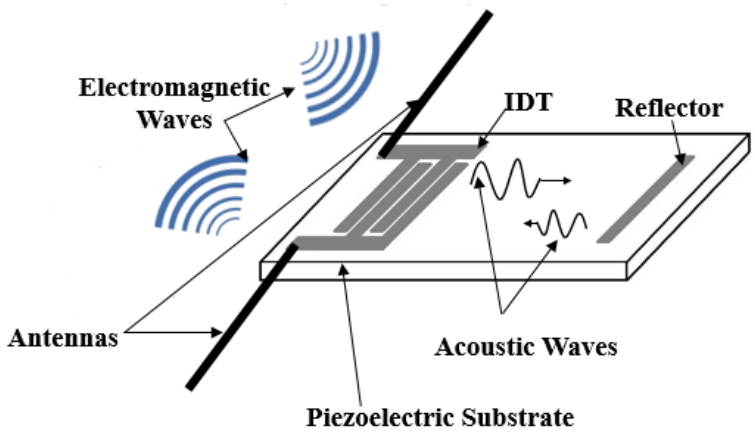

Figure 2.6: SAW Resonator operating principle illustration

A suitable model for the relationship between electrical and mechanical transduction in SAW resonators is the Butterworth Van Dyke (BvD) model [24, 25].

The model can be represented by the following circuit in figure 2.7

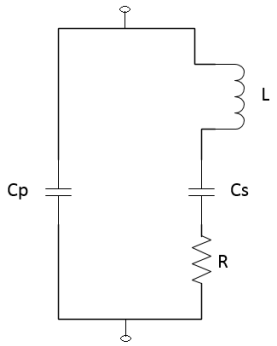

Figure 2.7: SAW resonator equivalent circuit, according to the BvD model [24,25]

The circuit behaviour approaches the exponential charging and discharging of a SAW resonator connected to to a dipole as a load. The BvD equivalent circuit consists on a RLC circuit in parallel with a capacitance C_p, which represents the transducer capacitance.
The exchange between elastic potential energy of deformation and kinetic energy, associated to particle motion from the surface wave resonance, are modelled by the inductance L and the capacitance C_s, respectively.
Simple circuit analysis reveals that the input admittance seen at the terminals of the circuit is given as [20]:

$$Y_i(\omega) = j\omega C_p + \frac{1}{R + j(\omega L - 1/\omega C_s)} \tag{2.1}$$

From this expression, we obtain approximated results for the natural resonant frequency f_r(maximum admittance), and the anti-resonant frequency f_a(minimum admittance), by assuming that the term $j\omega C_p$ as negligible, as being given by [20]:

$$f_r = \frac{1}{2\pi\sqrt{LC_s}} \tag{2.2}$$

$$f_a = f_r(1 + \frac{C_s}{2C_p}) \tag{2.3}$$

The bandwidth (BW) and the quality factor (Q) are also given by [20]:

$$BW = \frac{R}{2\pi L} \tag{2.4}$$

$$Q = \frac{f_r}{BW} \tag{2.5}$$

In spite of these expressions, the peak of S_{11} is not directly related to the resonant frequency of the device, so the measurement of the S_{11} magnitude is not sufficient to obtain the resonant frequency of the device. Figure 2.8 depicts an example of a computed resonant frequency f_r,

anti-resonant frequency and reflection coefficient S_{11}, using theoretical values of $R = 31,6\omega$, $C_p = 5,17pF$, $C_s = 0,84fF$ and $L = 0,16mH$ from a SENSeOR sensor (SE AS10), in comparison to the S_11 parameter measured in a VNA (Vector Network Analyser) [20]:

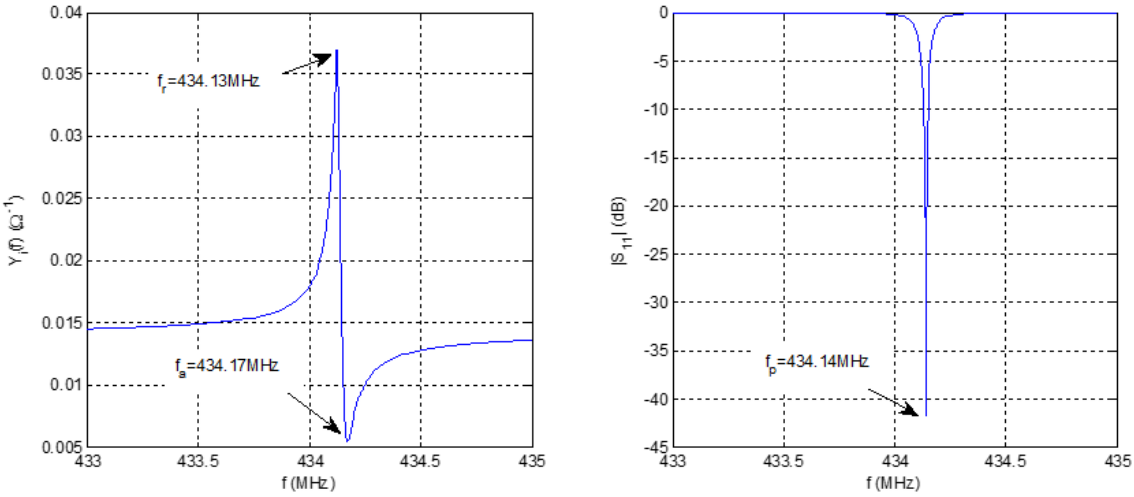

Figure 2.8: Example of computed resonant and anti-resonant frequency from a SENSeOR sensor

The approximation of f_p as the resonant frequency of the SAWR, generally does not introduce significant error in the measurements and allows a simpler measurement procedure.

2.2.1 Double SAW Resonators

When a SAW resonator is used as sensor, environmental variables affect the SAW in its propagation path, creating a relation between the resonant frequency and the environmental variables. Depending on the type of measurement one wants to realize with the sensors, different sensor design techniques can be employed to enhance or attenuate the environmental effects on the device response. Designing double SAW resonators (SAWDR) in a single piezoelectric wafer, instead of single resonators is a known way to more precisely manipulate the sensing device characteristics. For example, by enhancing devices temperature coefficients (TCFs) in temperature sensors (such technique is employed in the temperature sensors used in this work), or by making them cancel each other if one wants to remove the temperature effect on a measurement (two single resonators used in parallel, as a double resonance system in which the TCFs ideally cancel each other are used to measure strain in this work).
The frequency response of SAW double resonators is characterized by a double peak at the resonant frequencies of each individual SAWR, as can be observed in image 2.9, constructed from the data taken in a measurement of the reflection coefficient of one SENSeOR F162 temperature sensor realized in a Agilent E8361C VNA. The same measurement was performed with a single resonator WTS-2450B-3 temperature sensor from SAW Components, with resonance in the 2.45 GHz band(right image).

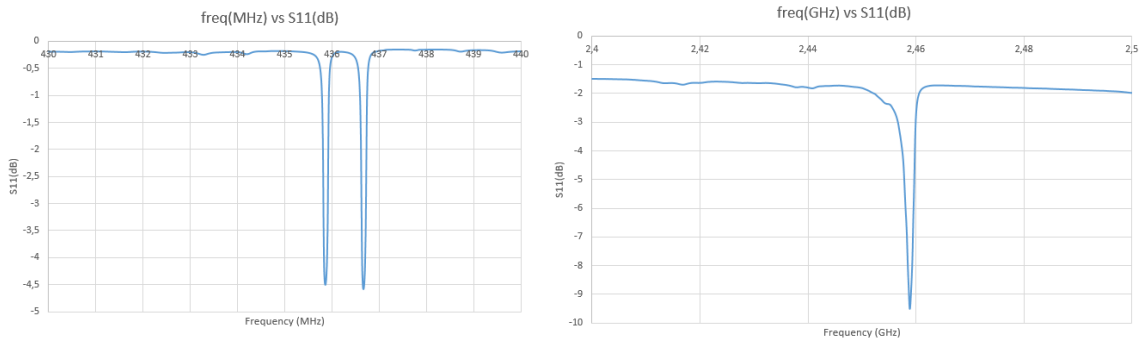

Figure 2.9: Example of a SAWDR resonant response, with a double negative peak (left) in comparison with a SAWR, with a single negative peak (right)

The environmental effects change the matching network of the resonators, causing shifting in both resonant frequencies. If the two resonators have different Q factors, and different impedance, the two sensors have different sensitivity to change in the matching conditions, which leads to a change in the distance between the two resonant peaks proportionally to the physical quantity being measured.
The manipulation of the sensitivity of this sensors to change in the matching conditions can be done using different methods: i) by connecting coupling inductors in parallel with the the resonators; ii) by varying the gap between the resonators; iii) by changing the thickness and number of IDT fingers; iv) by changing the IDT orientation in the material [26–28].
Image 2.10 illustrates two different topologies of SAWDR:

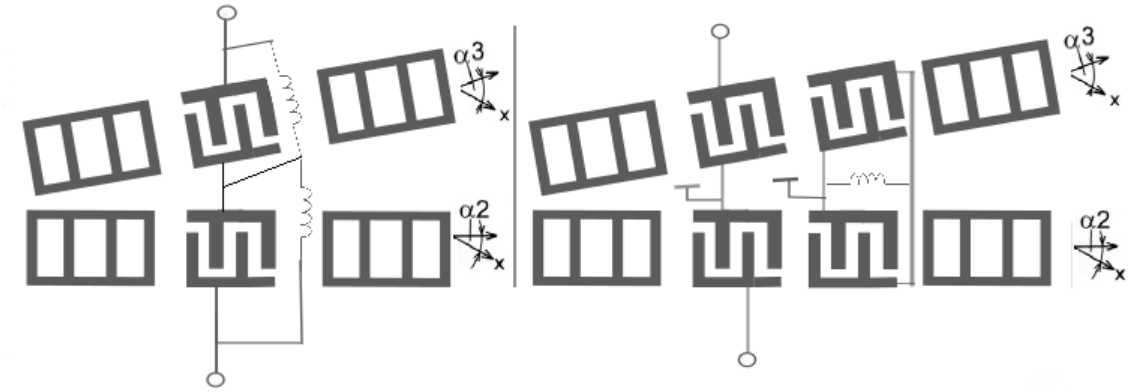

Figure 2.10: SAWDR as a serial connection of one-port resonators (left) and SAWDR as a parallel connection in a two- port resonator as presented in [28]

2.3 Interrogation Techniques

Changes in the resonance frequency of SAW resonators can be tracked with a read-out unit, using techniques similar to the ones employed by RADAR systems.

Depending on the sensor type, different interrogation techniques can be applied accordingly. For example, employing delay lines, the delay in time between request signal and the sensor response is a function of the measured physical quantity. Their interrogation is made in the time domain, since these are wideband devices. Resonators work in a well- known narrowband and can also be interrogated in the time domain, interrogating each single SAWR at separated periods of time. This method requires a bandwidth large enough to distinguish the signals and to guarantee orthogonality between them. Therefore, time domain interrogation usually needs faster electronics, which tends to be more expensive. For this reasons SAWR are usually interrogated in the frequency domain, since the excitation signal has to cover only the bandwidth of operation of the sensors being interrogated, meaning less energy, lower electronics cost and better resolution. [19,20].

2.3.1 Frequency Domain Interrogation

Frequency domain interrogation as previously mentioned, enables better measurement accuracy and resolution in multiple resonators interrogation. Similarly to RADAR techniques, interrogation and response are dealt separately and in the same way as in a VNA, with the sensor impedance being obtained as a function of frequency. The interrogation is realized using an excitation signal with an equally stepped combination of frequency tunes (sinusoids), and then the system monitors the response of each sensor and subsequently processes the information. A conceptual diagram of a read-out unit employing frequency domain sampling (FDS), is presented in figure 2.11

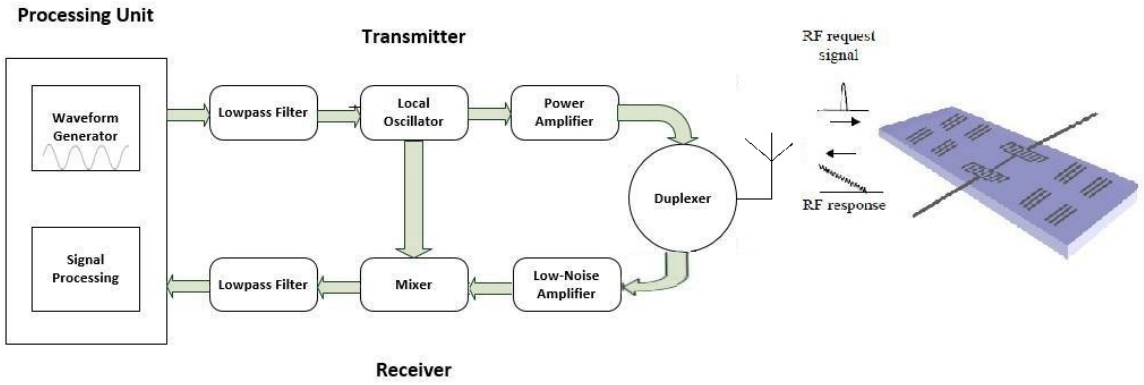

Figure 2.11: Diagram for a possible interrogation unit employing FDS, for SAWR passive sensing [20]

As transmitter the system starts by generating a sinusoidal wave form composed by different IF tones that, consisting in a combination of frequency tones, covering the device frequency band, which is sent to the sensor. The interrogation signal is usually synthesized using direct digital synthesis (DDS). Using a digital signal processor the signal is generated, in a baseband that is not the required interrogation band and is posteriorly converted into analogue domain

using a DAC. Afterwards, the signal is low- pass filtered to prevent aliasing effects and then up- converted to the frequency band of interest. The up- conversion is realized to reduce the DAC requirements.
Once in the RF ISM band, which is the band of interest, the signal is amplified and transmitted. The output of the PA, which to simplify can be fed by the Local Oscillator(LO), is connected to a duplexer, that works as RF switch by separating the transmission channel from the reception channel linked with the antenna.
The read-out unit switches to listening mode, and starts acting as a receiver and after some time delay due to internal reflection, typically some μs, receives the response signal from the sensor, from which, the reflection coefficient S_{11} is measured and the sensor input admittance is indirectly obtained. The resonance frequency can then, be more precisely estimated by association to the maximum input admittance value, near the sensor operation bandwidth.
Once the read- out unit catches the SAWR response signal, at first it feeds the LNA and is amplified to overcome the strong attenuation, suffered along the path (free space) and at the resonator substrate. After being amplified the signal is down- converted from the ISM band to baseband, at the Mixer using the LO tone, to reduce the requirements of the ADC. Finally, the signal is low- pass filtered to reduce the response distortion and to eliminate spurious high frequency content and the image signal, caused by down- conversion and then, the signal is sampled and converted to the frequency domain, using Fourier Transform.
Now that the signal is digitized, it is passed to the a processing unit for further digital processing, with the objective of improving resolution and accuracy, when the resonance frequency obtained is translated to the nominal value of the physical quantity, according to the sensor dynamics characterization.

2.3.2 Interrogation Limitations

There are bandwidth limitations of the read-out unit, which are related with the hardware limitations and with the sensor characteristics. The bandwidth limitations related to the sensors are associated with the duration of the interrogation signal, with the number of sensors being interrogated and the overall shared bandwidth, so the time of the interrogation-response cycle, is defined by the interrogation bandwidth, the processing time and the frequency resolution.
The possibilities for the excitation signal design are various, however the design of discrete swept sinusoids and multisines is a common choice, since they can be generated and recorded very efficiently for systematic measures. This type of signal accurately represents the complex nature in terms of amplitude, phase and bandwidth of modern telecommunications signals [20,29,30].
Discrete swept-sinusoids can be described by [20]:

$$s(t) = \sum_{k=1}^{N} a_k cos(2\pi f_k t) rect(f_k(t - \tau_k)), \tag{2.6}$$

where f_k is the k^{th} frequency sample of interest, with amplitude a_k, limited by a rectangular pulse (rect), centered at t= τ_k and with $1/f_k$ seconds of duration and:

$$\tau_k = \frac{1}{2f_k} + \sum_{p=1}^{k-1} \frac{1}{f_p}. \tag{2.7}$$

The Fourier Transform of such a signal is given by:

$$S(k) = \frac{a_k}{2f_k} e^{j2\pi f \tau_k} \left[e^{-j2\pi f_k \tau_k} \left(\frac{f - f_k}{f_k} \right) + e^{j2\pi f_k \tau_k} \left(\frac{f + f_k}{f_k} \right) \right]. \tag{2.8}$$

The result is a continuous spectrum between the frequencies of interest, with each component amplitude inversely proportional to f_k.

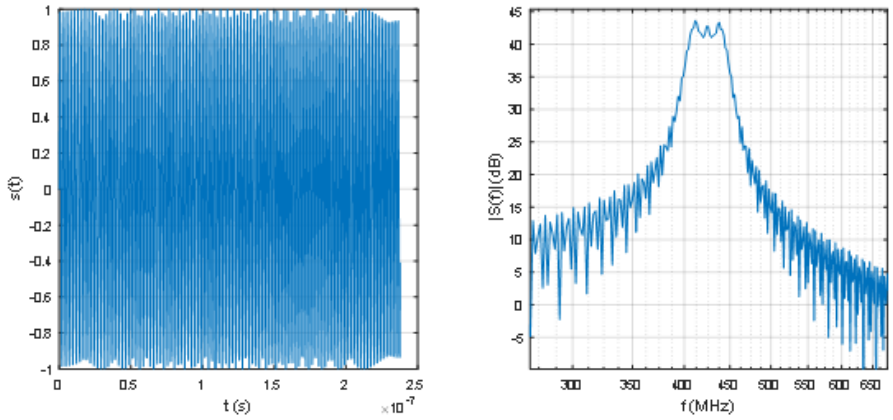

Figure 2.12: Discrete swept sinusoidal signal, in time and frequency domain representation respectively [20]

Depending on the SAW device behaviour, namely the time it takes to reach the steady state condition, the use of an interrogation signal with more than one period for each frequency tone may be important, which for N periods, will increase the rectangular window needed and the interrogation period by the same amount. For wider bandwidths and higher frequency resolutions this may be a problem, since it can originate too large interrogation times. The alternative is the use of Multisine signals.
Multisines are composed by a sum of several simultaneously generated frequency tones and can be described by the following equation:

$$x(t) = \sum_{k=1}^{N} A_k cos(\omega_k \theta_k) rect(\frac{t}{T_i}) \tag{2.9}$$

where A_k and θ_k, are the amplitude and the phase of the k^{th} sinusoid, in a total of N sinusoidal tunes. $\omega_k = \omega_0 + (k-1)\delta\omega$, is the k^{th} frequency tone, with ω_0 being the first and $\delta\omega$ the

constant frequency separation between consecutive tones. The Multisine signal is limited in time by the rectangular sinusoidal pulse of duration T_i. The period of a multisine signal is given by the inverse of the frequency resolution

$$T = \frac{N}{f_N - f_1} \tag{2.10}$$

where f_1 is the first frequency tone, f_N is the N^{th} frequency tone. The interrogation time is therefore, the number of periods considered to respect the steady state condition of the response, $T_i = TN_p$.
With the increase of the number of period cycles N_p in the interrogation, the rectangular window effect is attenuated, and the spectral content of the interrogation signal becomes increasingly as expected, composed by spectral lines at each tone that constitutes the signal, instead of the continuous spectrum verified for the discrete swept signal.

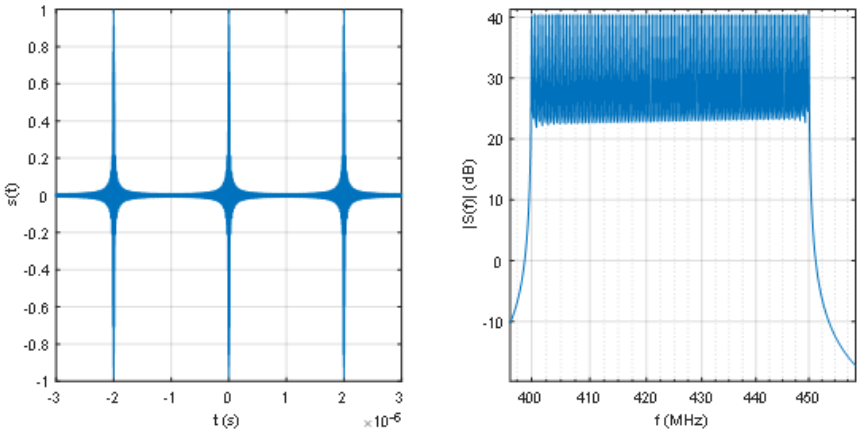

Figure 2.13: Multisine signal with more than one period, in time and frequency domain representation respectively [20]

The total time to interrogate the sensor T_t, must also consider the time taken by the read-out unit to process the received information T_{proc}, and the device delay response τ_D. So, considering N_p periods composing the interrogation signal, the total time T_t is given by

$$T_t = N_p(T_i + \tau_D + T_{proc}) \tag{2.11}$$

and the interrogation rate or system bandwidth R_i, is equal to $1/T_t$.
The read-out unit bandwidth limiting factors, are clearly exposed in equation 2.11, as they are defined by the hardware processing capabilities, the SAW device response speed and the duration of the interrogation signal that excites the SAW device.

2.3.3 Radio Link

For the radio link between the read-out and the sensor to work, there are several considerations that have to be carefully taken into account in the read-out unit design, given the sensor characteristics. All sources of errors and attenuations affecting the signal during the radio link must be considered to project a transceiver capable of generating a signal as "clean" as possible and that transmits an excitation signal with enough power. The response signal must have higher power than the receiver sensitivity, considering the desired SNR. The SNR of the signal must guarantee the information quality requirements.
From the errors affecting the radio request, their origin can come from the sensor itself, due to manufacturing, aging processes and bandwidth associated errors, for example, due to non-linearity in the direct dependence between the sensor and the measured physical quantity.
They can be originated by the interrogation system, associated with the system tuning or calibration parameters and it's capability to handle load changes without losing measurement quality. Or with phase noise due to distortion caused by non- linear intrinsic operation. The processes of up and down-conversion, amplification, sampling and digitation are intrinsically non- linear. Relatively to the digital converters (DAC and ADC) adequate choice, it is critical to guarantee the information accuracy, the resolution must be sufficiently wide, offset and gain errors adequately low. The SNR ratio of the ADC given by

$$SNR(ADC) = 6.02N + 1.76[dB] \tag{2.12}$$

where N is the digital converter Effective Number of Bits (ENOB), chosen considering a proper trade-off between cost and resolution.
The properties of the radio channel are also another factor to take into account, there is attenuation in the medium, if it is free space for example it's given by [19]

$$att = \left(\frac{4\pi d}{\lambda}\right)^p \tag{2.13}$$

where d is the distance, between the antennas and p=4 for bidirectional RF transmission. The noise power present in the channel, assuming a white stochastic process with Gausssian probability is equal to

$$P_n = KTB = -174[dBm/Hz] + 10log(BW) \tag{2.14}$$

where K is Boltzmann constant, and KT = -174 dBm/Hz is the Noise Density at ambient temperature, and BW the bandwidth. Interference between reception and transmission path is prevented with the choice of a proper RF switch, such as a duplexer or a circulator. Finally, other factors such as man made noise, errors due to the inherent imperfections of the sensors fixation to the mechanical set- up, in this case, to the rotation shaft and RF propagation fading must be considered.

Considering all error margins, attenuations and noise interferences explained before, a general expression for the RF Link Budget can be extracted [19]:

$$P_t = S_i + P_n + a_{sensor} + a_{path} + a_{switch} + M + F_{mm} + NF + SNR_0 - 10log(N)[dB] \quad (2.15)$$

where S_i is the receptor sensibility, P_n is the AWGN power, a_{sensor} is the sensor insertion loss, a_{path} is the path attenuation, a_{switch} is the RF switch insertion loss, M is the security margin for RF propagation fading and errors due to the sensor fixation to the set- up, F_{mm} is the margin given for man- made noise, NF is the reception system Noise Factor, SNR_0 is the Signal-to-Noise Ratio required, and N is the Number of Request Cycles stored at each interrogation.

2.4 Signal Processing Techniques

Once the SAW sensor response to the excitation signal is captured, the RF analogue signal is conditioned and then converted to the digital domain, employing Fast Fourier Transform (FFT) computation for improved efficiency. The sampling rate used must respect the Nyquist sampling criteria, meaning the sampling frequency must be over two times the maximum limit frequency of the bandwidth of interest. Next, the digital response signal is further computationally processed.
First, several response cycles are coherently averaged, to attenuate the random noise influence on the results. Then, to improve sampling resolution, processing techniques, namely, sample interpolation and signal windowing are applied. After this, using the mathematical tool of polynomial fitting, a new approximation for the peak value of the reflection coefficient response is obtained. From the peak value obtained with the previous steps, the input maximum admittance of the sensor is estimated from the mathematical model of the sensor behaviour and the resonant frequency value and consequently, the pretended physical quantity, can be extracted.

2.4.1 Signal Averaging

Averaging is the first processing step, after conversion from analogue to digital the response signal is stored in a processing register, being the number of samples stored at each response cycle given by the interrogation time T_i, divided by the sampling frequency *fs*. Coherent integration of the successive data streams is then performed, to reduce the statistical random noise of the response signal, therefore improving the SNR of the integrated signal.
The average of the received signals from N interrogation cycles is given by [19]:

$$r_N(t) = \frac{1}{N}\left(Nr(t) + \sum_{k=1}^{N} n_k(t)\right) \quad (2.16)$$

where, n_k is the additive noise at the k_{th} time sample.
Because the process is linear, there is no cross- correlation between signal and noise and cross-correlation between AWGN samples vanishes. The noise power is this way reduced by coherent integration and the signal SNR, or total energy for detection is increased by a factor of N. The mean noise power P_n is given by [20]:

$$P_n = \frac{1}{N^2} \sum_{k=1}^{N} \overline{n_k(t)^2} = \frac{\overline{n_k(t)^2}}{N} \tag{2.17}$$

At a sensing environment, susceptible to changes, such as the one under test in this work, with a fast rotating shaft, if there is signal amplitude variation during the interrogation, averaging may affect the signal power. In fact, given that the front end (directly mechanically affects SAW sensor) is a damped resonant system, the response after excitation might take a while to stabilize.
To solve this issue, it is recommended the use of excitation signals with multiple sinusoids of the same frequency, in the same interrogation stream, so the environment dynamics can be captured at a higher pace [19,31].

2.4.2 Frequency Domain Interpolation

The measurement of a discrete frequency spectra of an acquired signal usually comprehends, windowing of the signal samples and computing their discrete magnitude spectrum using Fast Fourier Transform. The resolution in the location of each individual frequency component depends on the number of samples, realized during analogue to digital conversion. The employment of frequency domain interpolation improves the resolution of the frequency spectrum of the acquired digital signal. The simplest form of interpolation consists of padding an appropriate number of zero samples at the tail of the discrete replica of the signal, equivalent to increasing the sampling frequency of the signal. FFT engines operating with split radix algorithm perform automatically the zero padding with an appropriate number of samples, always a power of two [20,32].
Better resolution can be achieved by fitting an interpolating parabola through the three largest consecutive spectrum peaks in the window of interest, and calculating the maximum of this parabola. In fact, interpolation efficiency can be significantly improved, depending on the interpolation technique employed and on the window formula applied to the sampled signal [33]. Further analysis on this interpolation techniques and windowing techniques and results obtained by employing them will be discussed in the following subsections.

2.4.3 Windowing

Signal windowing or truncation is a mathematical tool used to improve the frequency spectrum resolution of a signal.
The truncation of the signal if no special function is applied implies the multiplication by a

rectangular window. A rectangular window of length L, symmetrical with respect to t=0, has the following form:

$$w_r(t) = \frac{1}{L}\left(H\left(t+\frac{L}{2}\right) - H\left(t-\frac{L}{2}\right)\right) = \frac{1}{T} rect\left(\frac{t}{T}\right) \tag{2.18}$$

The Fourier Spectrum of the rectangular window can be described by

$$|W_r(f)| = \left|\frac{sin(\pi L f)}{\pi L f}\right| = sinc(Tf) \tag{2.19}$$

which the takes the following graphical form:

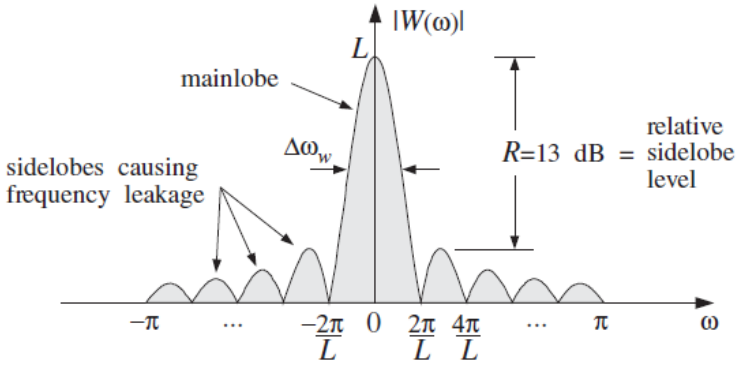

Figure 2.14: Rectangular Window Fourier Spectra representation as in [34]

The sidelobes represent spectral leakage, a process of widening of the signal spectral components, associated with the signal discontinuities caused by the process of approximating a continuous time signal by a discrete periodic signal with sharp transitions associated to the window limits.
Spectral leakage which is very large in rectangular windows, can be reduced by application of better windows. Interpolation efficiency, FFT frequency measure and amplitude dynamics can also be improved with different windows [20, 33, 34].
Another window of interest is the Gaussian Window, described as

$$w_g(t) = w_r(t) e^{-\frac{t^2}{2\sigma^2}} \tag{2.20}$$

and it's Fourier Spectrum, is given as

$$|W_g(f)| = \sqrt{\frac{\pi}{2}}\frac{\sigma}{T} e^{-2(\pi\sigma f)^2}\left|erf\left(\frac{1+j4\pi\sigma^2 f}{2\sigma\sqrt{2}}\right) + erf\left(\frac{1-j4\pi\sigma^2 f}{2\sigma\sqrt{2}}\right)\right| \tag{2.21}$$

where σ is the standard deviation of the window with duration T and erf() is the standard error function.

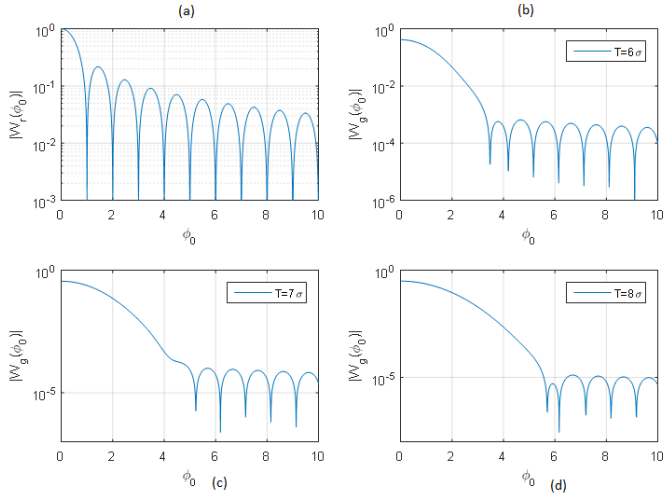

Figure 2.15: Comparison of the spectral properties of a rectangular window(a) and gaussian windows with different values of T (b),(c),(d) [20]

From observation of the previous figure, it is possible to conclude that, Gaussian windows have considerably less spectral leakage than the rectangular ones and that the width of the main lobe depends directly on the value of σ, factor which is taken into account in the window properties that will accommodate interpolation of the signal spectrum.

2.4.4 Fast Fourier Transform

Given that an utmost important part of the work being done is the estimation of the resonant frequency, there is a need to determine the relevant frequency components in the information acquired by the sensors measurements, by means of the frequency domain method of Fourier Transform. However, being Fourier analysis a method to operate in the continuous spectrum, since the referred analysis is done in the digital domain, Fourier transform is approximated by it's discrete version, the DFT, involving sampling and periodical replication in time. The DFT is mathematically described as

$$x(n) = \frac{1}{N_{FFT}} \sum_{k=1}^{N_{FFT}-1} X(k) e^{j\frac{2\pi nk}{N_{FFT}}} \tag{2.22}$$

$$X(k) = \sum_{n=0}^{N_{FFT}-1} x(n) e^{-j\frac{2\pi nk}{N_{FFT}}} \tag{2.23}$$

where $x(n)$ are samples of $x(t)$, taken at $t = nT_s$ and $X(k)$ are the spectrum frequencies of sampled signal $x(n)$, with $k = f/f_s$, each sample distanced to the next, in the frequency domain, by f_s/N_{FFT}, being f_s the sampling frequency and N_{FFT} the number of samples taken.

There are a considerable number of algorithms able to implement the computation of the

DFT (2.23), or its inverse, the IDFT (2.22), which both rely on the summation of samples multiplied by complex exponential terms, these algorithms are named Fast Fourier Transform (FFT) algorithms.
The number of samples and the number of operations performed determine the complexity of a given algorithm. The processing time considered in 2.11 is strongly dependent on how fast the FFT of input signals is performed. One of the fastest FFT algorithms is the split radix algorithm, which operates with a number of samples equal to a power of 2. The computational efficiency of FFT algorithms is usually specified by the number of operations necessary to compute the transform, for the split radix algorithm we have

$$O(N_{FFT}) = 4N_{FFT}log_2(N_{FFT}) - 6N_{FFT} + 8 \tag{2.24}$$

As the number of samples used increases, frequency resolution improves but the processing time necessary to compute the FFT of the sampled signal becomes larger, implying a tradeoff between the frequency domain resolution and processing speed one pretends, when designing or choosing a system for signal acquisition and processing. In the particular application of a processing unit for a SAW readout, where the acquired signal is truncated, and the processing focus is given to a specific part of the spectrum and where frequency resolution can be explored, through interpolation techniques, an optimum number of samples to guarantee both computation speed and accuracy can be estimated using the following figure of merit [20]:

$$FOM = O(N_{FFT})O(\epsilon) \tag{2.25}$$

where $O(N_{FFT})$ is the FFT algorithm complexity and $O(\epsilon)$ a term depending on the frequency estimation error, that will be described in the next subsection.

2.4.5 Interpolation Methods for Resonant Frequency Estimation

From the acquired Fourier spectra of both the interrogation and response signal, it is possible to obtain the reflection coefficient $S_{11}(k)$ of the sensor and its corresponding admittance response $Y_i(k)$. The index k defines the relation between sampling frequency f_s and real frequency as

$$f_k = \frac{k}{N_{FFT}} f_s \tag{2.26}$$

The DFTs of the interrogation and reflected signals are, respectively

$$\boldsymbol{S_i(k)} = S_i(k)e^{j\varphi_i(k)} \qquad and \qquad \boldsymbol{S_r(k)} = S_r(k)e^{j\varphi_r(k)} \tag{2.27}$$

Assuming that both transmitting and receiving antenna port are properly matched to the characteristic impedance, the reflection coefficient response is given by the ratio between the

reflected and transmitted waves:

$$\boldsymbol{S_{11}(k)} = \frac{\boldsymbol{S_r(k)}}{\boldsymbol{S_i(k)}} = \frac{S_r(k)}{S_i(k)} e^{j[\varphi_r(k) - \varphi_i(k)]} \tag{2.28}$$

The input admittance can be then computed from the reflection parameter, using the following expression

$$\boldsymbol{Y_i(k)} = \frac{1}{Z_0} \frac{1 - S_{11}(k)}{1 + S_{11}(k)} \tag{2.29}$$

It is reasonable to extract the resonant frequency from S_{11} data, if the antenna matching impedance falls into the range of impedances comprehended between the resonant and anti-resonant frequencies [20]. This method can simplifies the hardware and considerably reduces processing time.
However, since the peak in the S_{11} response corresponds in fact, to the best matching condition of the device and is not really representative of its resonant frequency. The inferred S_{11} value changes accordingly with the matching impedance applied, meaning that if adaptation is not appropriate an error is being committed by inferring the resonant frequency from S_{11}. The effect of matching the device simulated in figure 2.8 with different characteristic impedances comprehended between 10Ω to 90Ω, is demonstrated in figure 2.16:

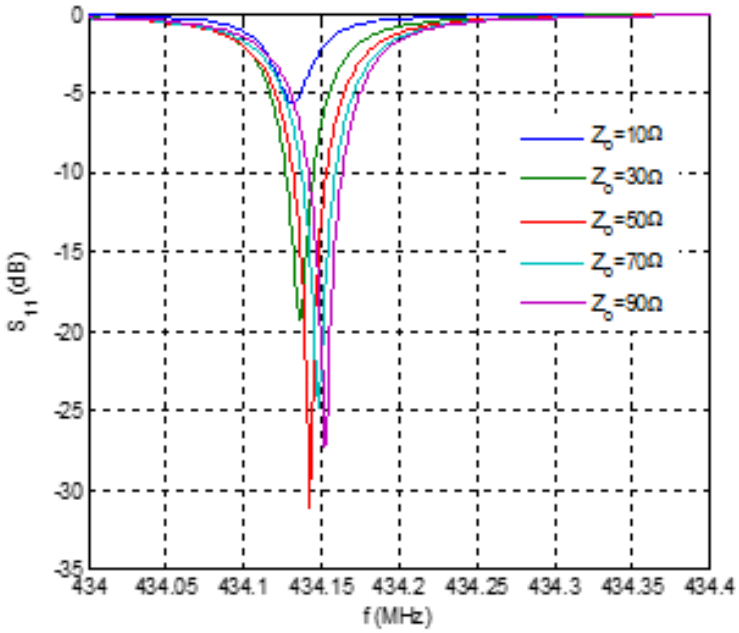

Figure 2.16: Example of the sensor's S_{11} dependence with the antenna matching impedance Z_0, as presented in [20].

Reconstructing Y_i from S_{11} after applying interpolation to a reduced set of Y_i samples near region of interest, delivers a more accurate resonant representation of the sensor and allows

to estimate the resonant frequency with more relaxed matching conditions [20].
The resolution gain in the determination of the resonant frequency can be enhanced depending on depends on the interpolation method applied to a determined data window and its number of points.
To perform interpolation methods such as Polynomial or Gaussian interpolation a data- set with a minimum of three points is needed. The Gaussian window the most appropriate as was already referred.
Assuming a consecutive set of three data points near the frequency peak, where k_m is the index of the maximum magnitude node of the discrete spectrum. By fitting a second order polynomial interpolation parabola such as

$$S_p(\varphi) = a(\varphi - \varphi_m)^2 + h \tag{2.30}$$

where φ is the normalized continuous frequency variable, given by

$$\varphi = \frac{f}{\Delta f} = \frac{N}{f_s} f = NT_s f = Lf \tag{2.31}$$

where L is the window length and N the number of samples.
An approximation of the abscissa of the parabolic interpolation maximum f_{in}, is given through nodes $S[k_m - 1]$, $S[k_m]$ and $S[k_m + 1]$ as [20,33]:

$$\varphi_{in} \cong \varphi_m = k_m + \Delta_m = k_m + \frac{S[k_m + 1] - S[k_m - 1]}{2(2S[k_m] - S[k_m + 1] - S[k_m - 1])} \tag{2.32}$$

and the obtained associated error is given by,

$$E(\varphi_d) = \varphi_m - \varphi_{in} = k_m + \Delta_m - \varphi_{in} = \Delta_m - \varphi_d \tag{2.33}$$

where $\varphi_d = \varphi_{in} - k_m$.
Given that $W(\varphi_d + n) = S[k_m - n]$, with $n = -1, 0, 1$ and substituting 2.32 in the previous expression, it can be rewritten as [20,33]:

$$E(\varphi_d) = -\frac{W(\varphi_d + 1) - W(\varphi_d - 1)}{2(2W(\varphi_d) - W(\varphi_d + 1) - W(\varphi_d - 1)} - \varphi_d \tag{2.34}$$

On the other hand, a Gaussian interpolation curve is mathematically described as

$$S_g(\varphi) = exp(a'(\varphi - \varphi_m)^2 + h') \tag{2.35}$$

which represents a parabola in the logarithmic scale. Gaussian interpolation can be derived

from the parabolic interpolation expression 2.32, using the logarithmic spectrum values, as follows

$$\varphi_{in} \cong \varphi_m = k_m + \Delta_m = k_m + \frac{ln\left(\frac{S[k_m+1]}{S[k_m-1]}\right)}{2ln\left(\frac{S[k_m]^2}{S[k_m+1]S[k_m-1]}\right)} \tag{2.36}$$

with an associated error of,

$$E(\varphi_d) = -\frac{ln\left(\frac{W(\varphi_d+1)}{W(\varphi_d-1)}\right)}{2ln\left(\frac{W(\varphi_d)^2}{W(\varphi_d+1)W(\varphi_d-1)}\right)} \tag{2.37}$$

with $\varphi_d = \varphi_{in} - k_m$.
The metric for performance evaluation of a given interpolation method, is the interpolation gain, which defines the ratio between the largest frequency error without and with interpolation, defined as

$$G = \frac{\Delta_f}{2max|E(\varphi_d)|} \tag{2.38}$$

According to [34] and [33] Gaussian windowing provides the better approximation, since it has the minimum error approximation and the maximum gain factor.

Chapter 3

MECHANICAL TEST SET- UPS AND EXPERIMENTAL PROCEDURES

Figure 3.1 illustrates the general architecture employed to measure torque in a rotating shaft

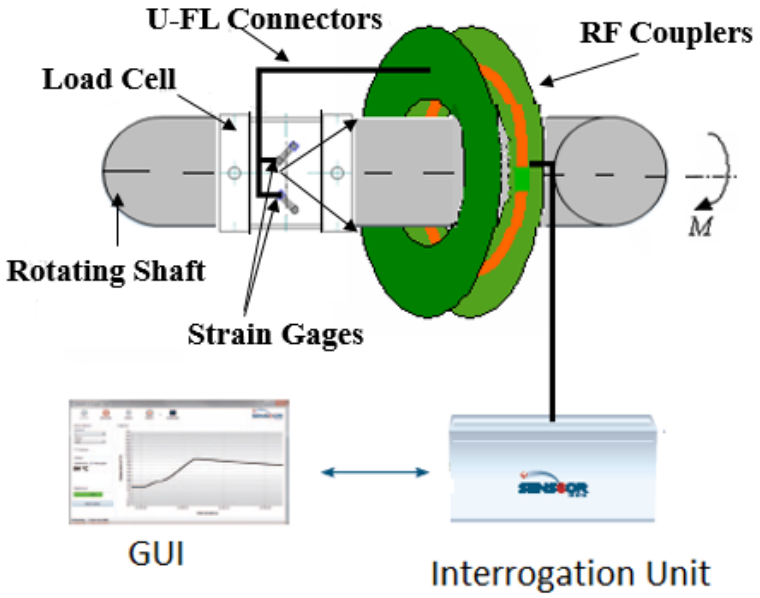

Figure 3.1: Measurement of applied torque in a rotating shaft using SAW strain sensors

So far in this work, it was made a review on SAW technology and some of its applications, with more emphasis on the description of the electrical behaviour and the material constitution of SAW Resonators.
After that, a synthesis on the interrogation techniques employed to extract information on this

sensors and its limitations was realized. A general description of the budget analysis performed when projecting a transceiver capable of effectively communicating with such sensors is also made.
Finalising the previous chapter is a survey, on the processing techniques used to improve measurement resolution once information is extracted from the SAW sensor.
In this Chapter, is given a complete description of the practical techniques and set-ups designed and assembled in order to characterize and validate the commercial solutions employed in this work. First, the load cell in which the sensors and the rotor antenna are fixed is presented. Then, the motivations and details behind the construction of the RF rotary coupler antennas needed for rotational measurements are addressed. Next, the motivations behind the set- ups are explained by analysing the details of their assemblage and by explaining how torque is measured in them. The chapter will be ended with a description of the practical tests employed in order to materialize the work objectives. In figure 3.2 the physics descriptive of the torque generated due to the application of strain in a solid cylindrical bar are illustrated:

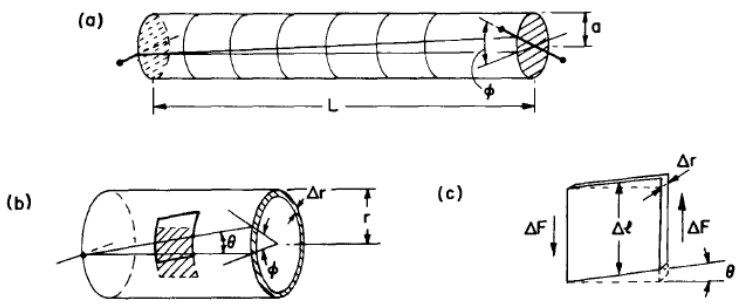

Figure 3.2: (a)Cylindrical bar in torsion. (b)Cylindrical shell in torsion. (c)Each small piece of the shell is in shear. [35]

The torque applied to a shaft with length L and radius a, is proportional to the angle ϕ, by which both ends of the shaft are twisted 3.2(a). To calculate torque applied, we can think of such an object as being composed by infinitesimal cylindrical shells of thickness Δr 3.2(b), suffering from a contribution of the torque applied to the whole shaft. Each shell is made of infinitesimal small square elements, that due to torsion are distorted into parallelograms 3.2(c). The shear angle of each of these elements is

$$\theta = \frac{r\phi}{L} \tag{3.1}$$

and the Shear Stress in the material is the tangential force ΔF on the end of the parallelogram divided by the area ΔrΔl

$$g = \mu\theta = \mu\frac{r\phi}{L} = \frac{\Delta F}{\Delta r \Delta l} \tag{3.2}$$

The torque contribution of the tangential force ΔF, around the axis of the rod is given by

$$\Delta\tau = r\Delta F = rg\Delta l\Delta r \tag{3.3}$$

Applying 3.2 and integrating the torque contributions around the whole circumference of the cylinder(Δl between 0 and 2πr), and considering the sum of the torque of all infinitesimal concentric cylindrical shells (integrating Δr between 0 and a), we obtain the total torque applied to the rod as [35]

$$\tau = \mu\frac{\pi a^4}{2L}\phi \tag{3.4}$$

The previously deduced formula can be related to formula 4.11, given to extract the torque applied to a shaft using the acquired sensors.
This values of torque are extracted by measuring strain applied in a load cell in which the sensors were fixed. The load cell was designed by AST Coimbra, technical advisers in the RTMGear Project. The cell consists in a shallow cylinder fabricated in aluminium Al7075-T6, designed in order to support without deformation, torque in the order of the 250 Nm. The fabricated schematics were the following:

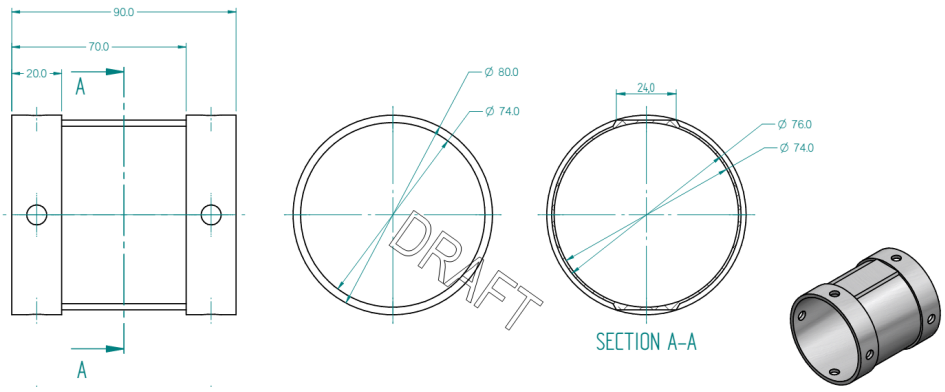

Figure 3.3: Schematic of the Load Cell employed during the experiment

3.1 Large Diameter RF Rotary Coupler

A dipole antenna is the simplest choice to assure communication in the 433 MHz band. However, this solution compromises the communication between the rotor and stator antenna for all the 360º of the rotation. In order to establish stable communication between the sensors and the interrogation unit RF rotary couplers were used. The requirements for a good RF rotary coupler are a flat frequency response, small angular variation of the measured resonant frequency and of the insertion loss [36].
The first RF rotary coupler design with the objective of measuring torque using a SAW sensor was patented by Racal, Ltd., UK in 1996 [37] and is called the Racal Coupler, who was concluded to be adequate for low circumference diameters, with length given by $\simeq \lambda/4$, with the

disadvantage of haven transmission nulls for determined orientation angles, which degraded the communication.
An alternative, topologically identical, RF coupler for length diameters to the order of $\simeq \lambda/4$ and beyond, that resolved the problem of the transmission null points presence, but with significant insertion loss for a length equal to λ, was proposed by Transense in [36].
A badly designed RF coupler can result in excessive attenuation of the signal or the introduction of systematic errors, difficult to control that might compromise the system accuracy, as it's been shown in [38]. That being said, it's important to guarantee, when designing a RF coupler based on microstrip lines, that the line width and length meet the shaft and stator diameter, but also take into account the wavelength of the transmitted signals.
In order to reach larger diameters, such as the ones needed in the context of this work the topology applied was the Large Diameter Coupler. This topology uses a matched termination of 50 Ω on a $n * \lambda$ diameter stator, employing the travelling wave regime to minimize the amplitude variation of the signal along the stator circumference. The rotor line is of $\lambda/4$ length and short- circuited at one of its ends. The stator line length can be of multiples of the wavelength, $Lc = n\lambda$. The width of both stator and rotor microstrip lines is designed to match the aimed characteristic impedance. This topology adequacy for gaps above 4mm between the two coupling lines is the reason for it's choice as the antennas connected to the read- out unit at the stator and sensor at the rotor. An example of application of this topology is presented in [7]. The topology is illustrated in figure 3.4.

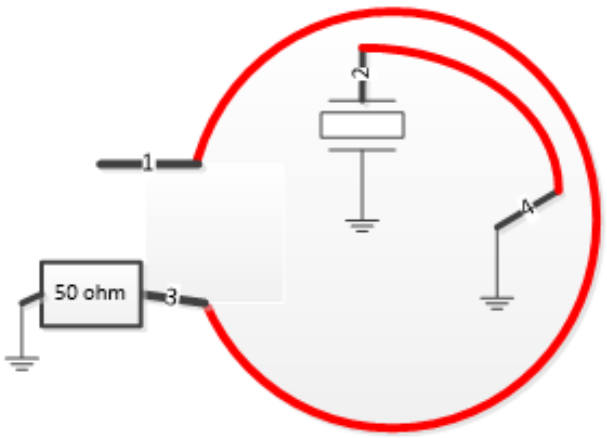

Figure 3.4: Large diameter coupler topology as presented in [36]

Due to the SAW resonator high selectivity in its frequency response, a single RF Coupler line can be connected to multiple sensors in parallel, care its only needed when choosing the resonant frequencies of each, making sure that they don't overlap.
The dimensions of the load cell on which the sensors are fixed, demand for a rotor Coupler design with approximately 42 mm radius. This means that, the stator Coupler to be mounted around the load cell demands a minimum perimeter of 263,7 mm.

The designed solution by the RTMGear work group at the Institute of Telecommunications of Aveiro, consists in a microstrip line made of FR-4 subtract, with a copper conductor and a dielectric constant of 4,5, with $H = 0,8$ mm of height and width $W = 1,5$ mm. The Rotor ($\lambda/4$) substrate has length $L = 93,86$ mm, while the Stator(λ) substrate has length $L = 375,44$ mm.
Due to the maximum diameters stipulated for the couplers, as previously defined, the coupler to be assembled on the stator was drawn in a shape of a saw.
The designed couplers are presented in the following image:

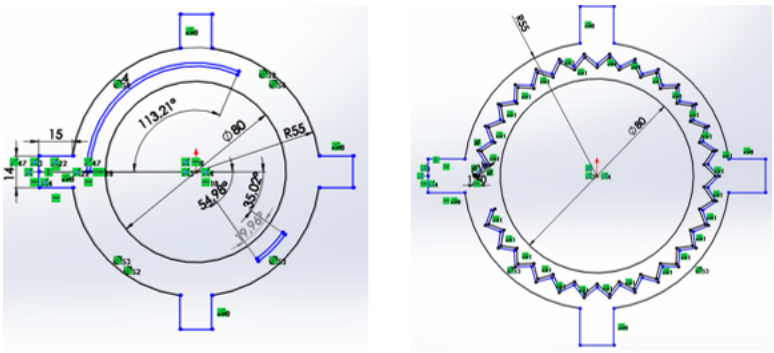

Figure 3.5: Schematic of the projected RF rotary couplers

The longer microstrip line was designed for the test frequency of 433MHz and the shorter for 2.45G.
The manufactured coupler was composed by two non-conductive flat rings; one ring was physically attached with epoxy to the load cell (rotor) and the other ring was attached to a metallic L-shaped piece with screws (stator). This L-shaped piece was attached with screws to a metallic base. The experimental assembly is shown in figure 3.6

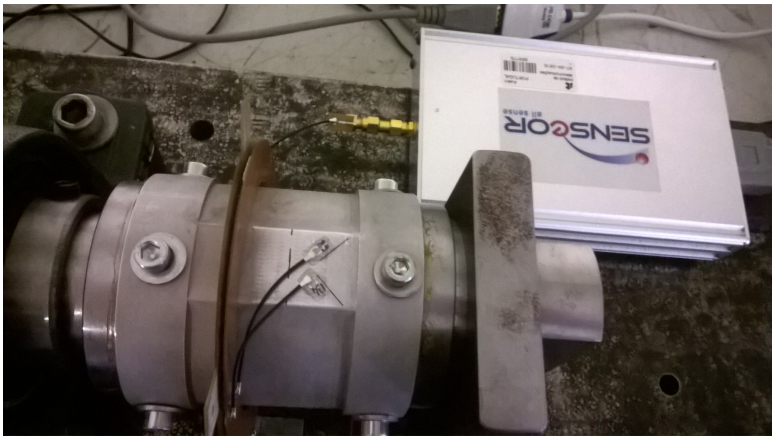

Figure 3.6: Load cell with the sensors attached and the RF Coupler positioned for measurement

Transmission lines on the surface behaved as the antenna. The other surface was covered with a copper layer acting as a ground plane. Both the stator coupler is connected to the interrogation unit and the rotor coupler to the sensors using U-FL RF cables. The transmission lines were positioned face-to-face with approximately a 2 mm gap in between them.

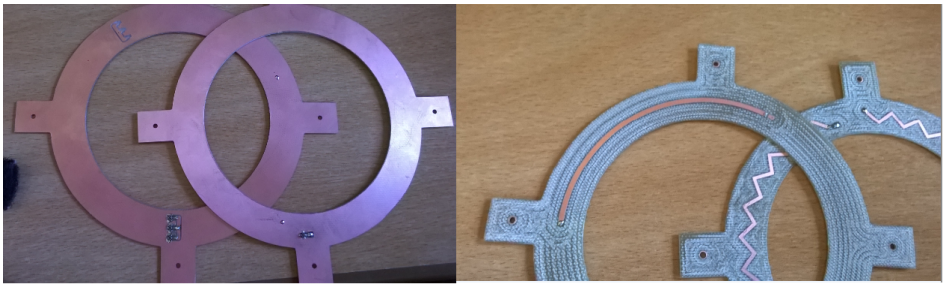

Figure 3.7: Manufactured Couplers used together with SENSeOR strain measurement kit

3.2 Mechanical Set- ups

In order to validate the use of SAW sensors to measure temperature and torque inside a power reduction gearbox, two mechanical Set- ups were designed and assembled with the technical assistance of the Mechanical Engineering students Francisco Felício, João Pereira, António Ramalho, Bernardo Fernandes and Engineer Ricardo Beja, under the supervision of Professor António Bastos of the Mechanical Engineering Department of the Aveiro University. Two mechanical set- ups were assembled. One set- up was used for static measurements and the other for dynamic rotation measurements. In the Static Set- up the calibration curves of the SAW strain gages were extracted. In the Dynamic Set- up experiments to evaluate the speed and temperature effect on the SAW sensors uncertainty and to perform torque and temperature measurements were realised.

3.2.1 Static Set- up

The static test Set- up assembled consisted on a shaft fixed at one end and attached to a movable arm on the other end, as depicted in 3.8. The load cell containing the sensors was screwed on the shaft, which in turn is supported by two bearings.

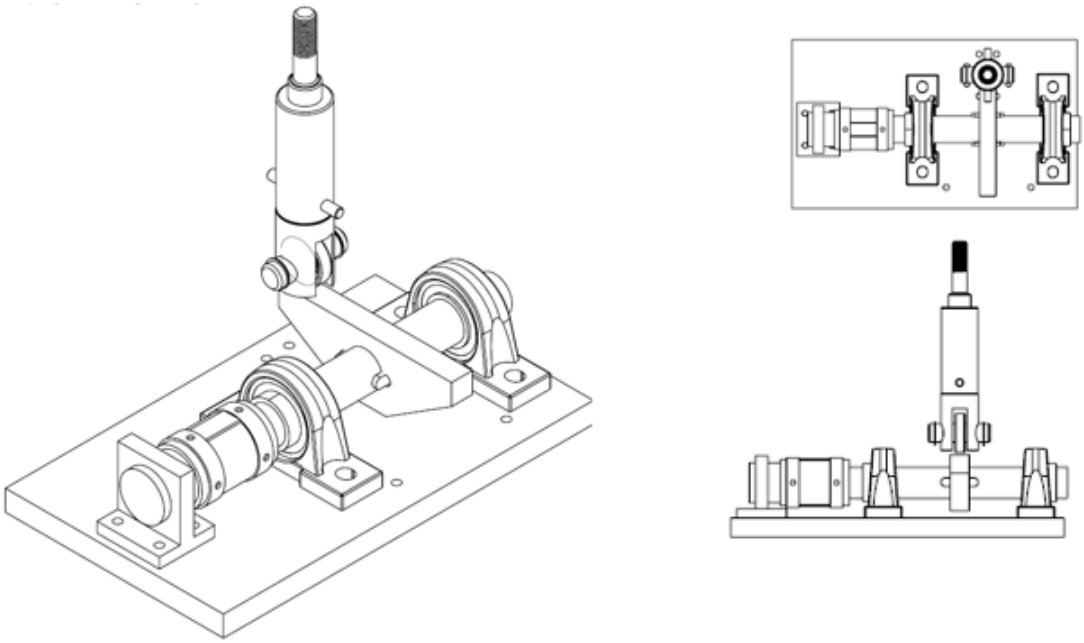

Figure 3.8: CAD schematic of the Static Set- up employed in the strain calibration curve

Using a universal test machine Shimadzu Autograph AGS-100kN, various force values were applied perpendicularly on the moveable arm, that is connected to the steel shaft. This force translates into a torque value applied to the shaft, given by the following expression:

$$M = F\frac{L}{2}sin\theta \approx F\frac{L}{2} \tag{3.5}$$

where M is the torque, F is the force applied by the universal test machine, L is the length of the moveable arm and θ is the angle between the applied force vector and the arm longitudinal axis. Given that the maximum displacement measured by the universal test machine was of $\approx$ 1.4mm and half of L(distance to the arm axis) is 95 mm, based on that it is admissible the approximation of $sin\theta = 1$.
Since the load cell is made of hollow aluminium cylinder which is considerably more elastic than steel, the torque applied slightly deforms the load cell while the bearings support vertical forces, making the load cell sensible to the applied torque.

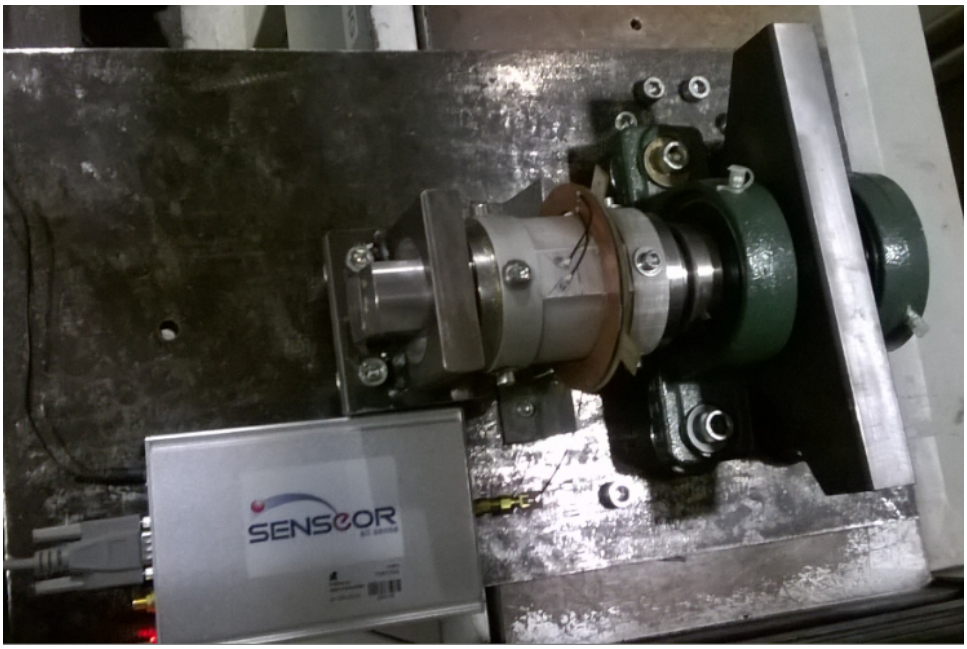

Figure 3.9: Static set- up test bench assembled

3.2.2 Dynamic Set- up

The CAD designs of the dynamic set-up are shown in figure 3.10. The assembled set- up is shown in figure 3.11 and is explained in detail next.

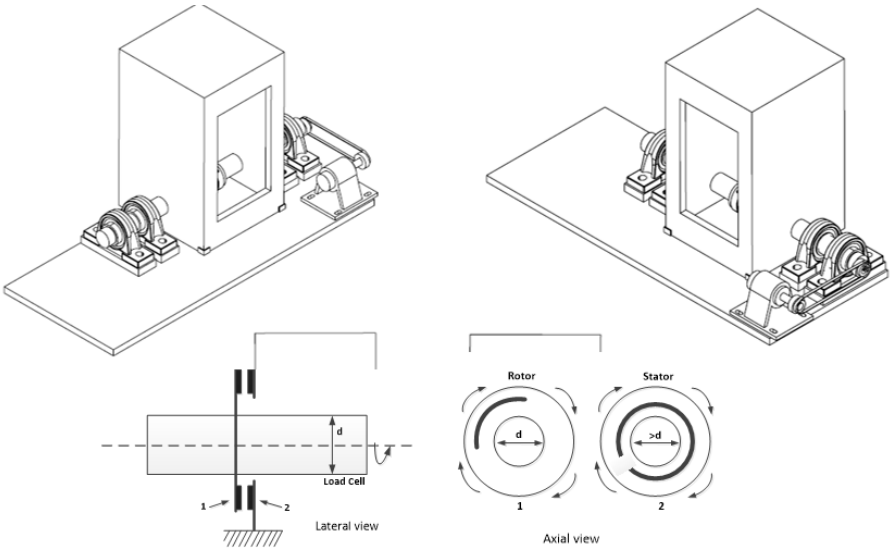

Figure 3.10: CAD schematic of the Dynamic Set- up employed in the rotation measurements

The set- up is constituted by a rotating shaft supported by two bearings, to which a cell containing the glued SAW strain gages and Rotor coupler antenna is screwed. The shaft

penetrates a commercial oven fixed to a metallic bench, perforated for this effect. Machined metallic parallelepiped were used to elevate the bearings to a position in which, the cell and antennas dimensions where guaranteed to fit and some margin for work manoeuvrability inside the oven was allowed.
The Stator antenna is fixed with the use of a machined metallic piece in the shape of "L", inside the oven, in a position where communication between couplers was guaranteed (with similar distance to the one used, in the coupler characterization tests of the following chapter). The AC motor used is a NORD SK80-LH/2, with a nominal rotating speed of 2820 rpm is connected to the shaft shaft through pulleys using a toothed belt. The motor is fixed in the downward plane of the board, since the positioning of the oven in the upward plane, would not permit the motor fixation in the same plane. The braking of the system is done by compressing the mobile piece, at the right of the assembly against the shaft. The torque obtained because of the braking system action is given by the following expression:

$$M = \frac{2}{3}\mu|\vec{F}|R \tag{3.6}$$

where F is the force perpendicularly applied on the brake disk, R the radius of the shaft (assuming the brake has contact with the whole circular area) and μ is the friction coefficient between the shaft and the brake disk.
On the right of the brake, is a frequency inverter NORDAC AC Vector Drive of the SK500E family, with 200-240 V 3-phased power supply, used to program the set- up rotational speed.

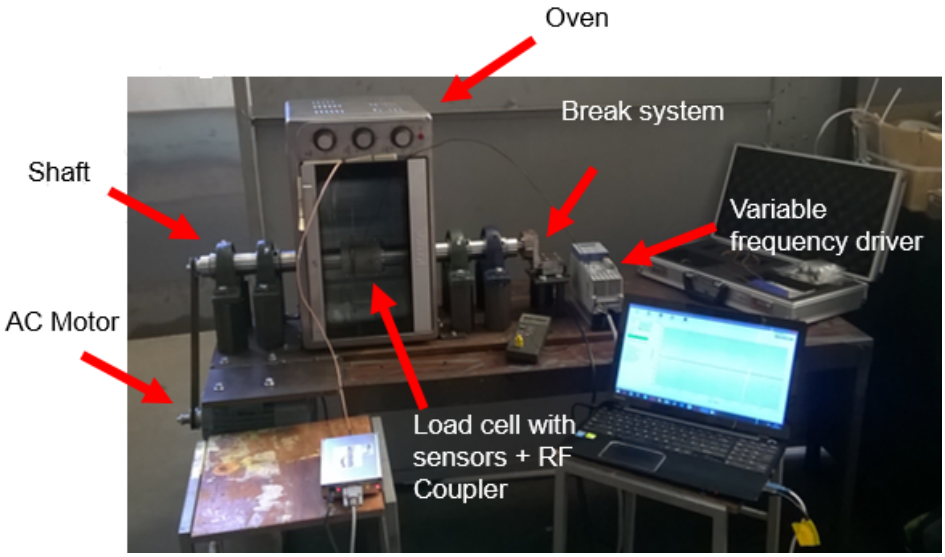

Figure 3.11: Dynamic set- up assembled, in order to perform tests with the objective of achieving use validation, for SAW strain gages in Torque measurements

The set- up configuration as it is was prepared for high rotation speed, however lacked

power transmission to perform the torque measurements. In fact, when the brake was applied to the shaft, a significant reduction in rotational speed was verified.
To perform torque measurements in a measurable range, the set-up previously presented suffered two major modifications, that are presented in figure 3.12. In the braking system initially proposed, the force made between the shaft and the brake pad was intended to be made by hand. However, after testing it was verified that the values of force made with this solution was below the range necessary to measure torque. As such, an upgraded braking system was installed. In this set up, the braking was performed by tightening a screw against a metallic piece before the load cell to guarantee the last was not damaged. The load cell was positioned there, to estimate the perpendicular force being applied. Connected to the load cell at the end of the mobile piece, was a brake friction material that would be pressed against the shaft. The friction coefficient of the brake pad can be estimated to be comprehended between $\mu = [0,45; 0,6]$ depending on the pad temperature, age and on its alignment with the shaft, however since a test to estimate this value with precision was not made the higher value will be used by default.
The initial pulleys were also substituted by pulleys with a larger diameter ratio between them to increase the power transmission between the motor and shaft. The specific diameter of the pulley connected to motor was $Dp_1 = 39,41mm$, while the pulley connected to the shaft plane had $Dp_2 = 291,06mm$. This modification meant that the torque generated at the motor was being transmitted and amplified by a factor of Dp_2/Dp_1, into the rotation shaft. The toothed belt connecting the pulleys was also substituted, being the new perimeter of 1249,8 mm. The change of the pulley imposed a slight modification in the motor position and a re- alignment in the whole system, before performing measurements.

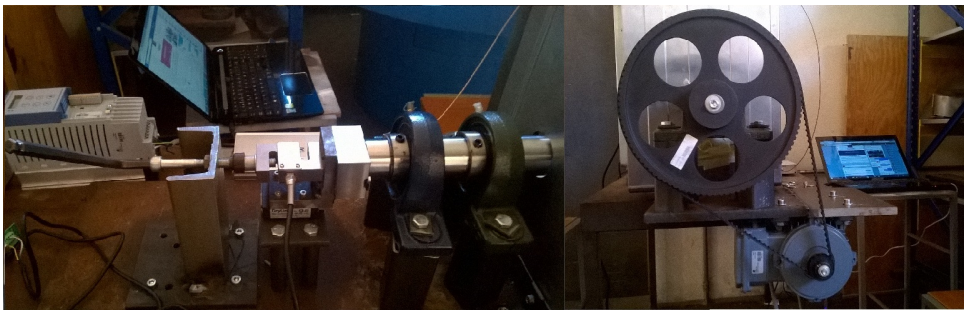

Figure 3.12: Dynamic set- up modifications realized to perform torque measurements: breaking system (on the left) and pulleys (on the right)

3.3 Practical Tests

In this chapter a description of the testing protocols followed performing measurements in the assembled set- ups. All sensor evaluation tests performed in a fabricated mechanical set-up were done under the supervision of Professor António Bastos.
In the experiments performed during this work, all sensors utilized were interrogated by the

SENSeOR wideband radio-frequency transceiver WR D005 shown in figure 3.13(left), whose dimensions are $18.4 * 10.9 * 3cm^3$. This unit operates in the 434 MHz ISM band [430.5, 449.5] MHz. It provides digital RS232/USB and analogue outputs. The data was extract and recorded into .txt files during the experiments using a sampling frequency of 10 Hz. The GUI has an options menu as shown in figure 3.13(right) in which the maximum allowed standard deviation in the extracted resonant frequencies accepted in an interrogation cycle is defined. The default value of 5 KHz was used in all tests except in the tests to determine the uncertainty caused by temperature and speed in the measurements, where a 3 KHz limit was defined. This tool can be used to attenuate error by filtering uninteresting (null) values that would deteriorate the data. Cubic spline interpolation to determine the extracted frequency values was also selected.

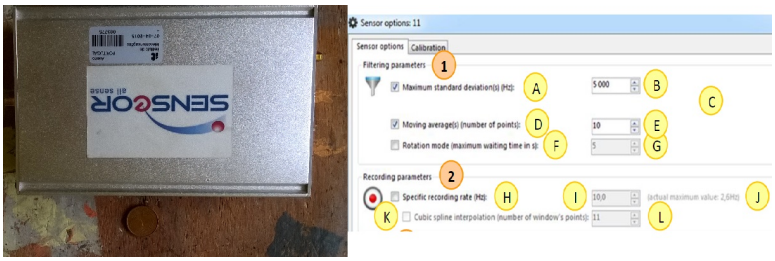

Figure 3.13: Read- out unit SENSeOR WRD005 utilized in the experiments performed(left) Options menu of the GUI(right)

The sensors available within the 433 MHz kit used in the measurements at hand, are the SENSeOR TSE F162 temperature sensor and the strain gages SSE E015 and SSE E016, shown in figure 3.14.

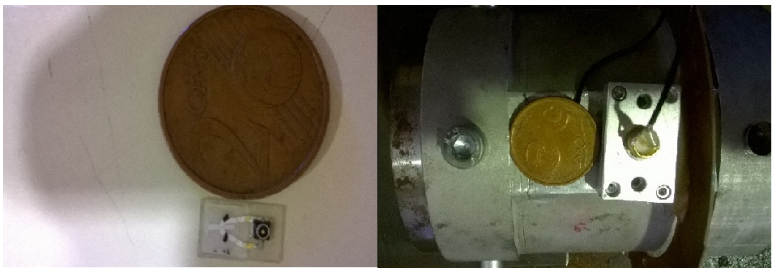

Figure 3.14: SSE E01x strain sensor(left) TSE F162 temperature sensor(right)

The fixation of the strain gages was performed accordingly to the recommendations given in the strain gages measurement configurations manual in order to measure torque, and the Instruction Bulletins of the manufacturers of other tools used in this task, such as the Micro-Measurements Certified M-Bond 200 Glue and the M-Bond 200 catalyst.
In each of the data vectors obtained the null values (communication failure) were removed and the mean result was applied.
The tests performed are described in the following subsections.

3.3.1 Coupler characterization tests

As has already been detailed, one of the critical points of this projects lies in the capability of the system to ensure a communication link, between the read- out unit and the SAW sensors applied in a rotating shaft inside an airplane gearbox, for all 360 °. This should be possible if the antennas connected to both the sensors and the read- out unit, were designed in a microstrip RF Coupler topology as displayed in 3.4.
Tests were run in order to analyse the coupler performance, where four variations of the original topology were tested, consisting in combinations of Stator coupler port 3 terminated with a 50 Ω resistor or a short- circuit, and Rotor coupler port 4 terminated also with a 50 Ω resistor or a short- circuit, designed for the test frequencies of 433 MHz and for 2.45 GHz.
The couplers were placed in a parallel position, distanced by approximately 2mm. Position in which after trial, it was concluded that communication was guaranteed.
In every trial, the S11, S21 and S22 parameters were measured in a test bench which allowed a rotation over the 360°. Samples were taken each 5°. It was observed during the experiment that S12 ≈ S22, was an appropriate assumption during the measures, given that differences between both parameters larger than 0.2 dB, were not observed in any measurement in the VNA Agilent E8361C.

3.3.2 Calibration for temperature measurement of the temperature and strain sensors

The measurements to obtain the temperature calibration curves were performed in a heating chamber ACS Challange 340, with a 2,5m^3 heating area, located in the second building of the Institute of Telecommunications of Aveiro. To measure a set of successive temperature points with reliability, a waiting time of 45 minutes between successive measurements was employed, for temperature stabilization.
The experimental set- up used is illustrated in figure 3.15:

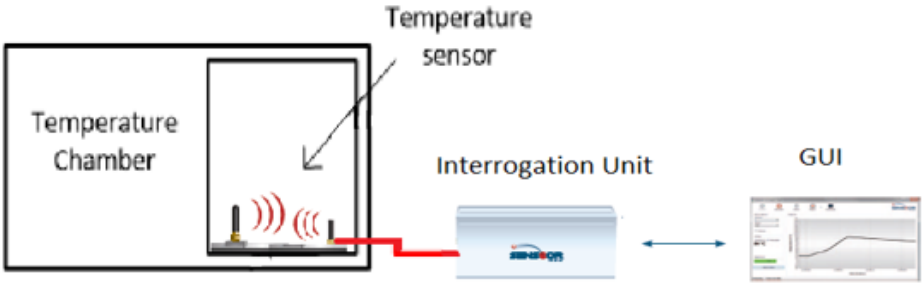

Figure 3.15: Set- up for the SENSeOR TSE F162 temperature sensor characterization measurements

The temperature measurements were performed in sets of 4 different scenarios, the first

employing measurements with the sensors and the SENSeOR interrogation unit connected to the dipole antenna available within the kit, and the remaining three scenarios using the RF large diameter rotary coupler, designed specifically to guarantee communication in referred working RF bands. There is a change of 120 º in the orientation between the coupler designed for the stator part of the gearbox and the rotor coupler, in each of three scenarios employing the RF couplers. The strain sensors calibration in temperature was performed for a single RF coupler orientation.
Using the recording capabilities of the interrogation unit data was extracted from temperature points stepped by 10º C, except the 25 º C which was also extracted, in the range comprehended between the 0º and the 80º C. The recording of each data set occurred during at least one minute.

3.3.3 Calibration for torque measurement of the strain sensors using the static set- up

The calibration curve relating strain measured and the resonant frequencies of the sensors, was obtained using one Shimadzu Autograph AGS-100kN Testing Machine, at ambient temperature. The machine was programmed to increase the force values applied perpendicularly on the moveable arm, that is connected to the steel shaft, incrementally and recording those same values, while at the same time the interrogation unit was extracting resonant frequency data. The sampling frequencies of both machines were integer multiples and the data was obtained by crossing both logs.
The following figure exemplifies the procedure in both directions. Downward by forcing the machine arm against the set-up moveable arm. In the opposite direction by attaching the moveable arm to the universal test machine and pulling the moveable arm up.

Figure 3.16: Experiments realized to obtain the SENSeOR SSE E015 and SSE E016 calibration cuves: (a) Load cell torsional force applied in the downward direction (b) Load cell torsional force applied in the upward direction

3.3.4 Testing the uncertainty introduced by high rotation speed and temperature in the measurements

The SAW sensors uncertainty evaluation was performed in a series of tests with the intent of understanding the effect of factors like temperature and speed in the measurements. For the effect, data logs were extracted from the sets of measurements at three different temperature values of 25 ^{o}C, 47,5 ^{o}C, 60 ^{o}C. The measurements were realized in the dynamic set- up, to stabilize the temperature set points inside the oven, at least 30 minutes of waiting time for heating were given.
Data logs were extracted for a duration of at least two minutes, at the different set points, considering the data frame acceptance registered at the time, in order to have at least 1000 valid data points at each data log. This number of data points per log can be considered statistically relevant.
The rotation speed was determined by programming the frequency inverter with a value comprehended between $f = [10 : 40]$ with a step of 5 between successive points and given by the expression:

$$\frac{2820}{50} * f \tag{3.7}$$

where f is the frequency programmed on the frequency inverter. The maximum programmed value used during the experiment was $f = 40$, given that at superior speed values the set- up vibration was considerable and could affect the results accuracy.
A digital thermometer using a thermocouple type J, was used to perform set point temperature value and a digital tachometer HS2234 was also used to determine the real rotation speed of the shaft during the data extraction, for simplicity and accuracy reasons. Since the glass door of the oven had a significant aperture, the thermocouple and the RF cable connection between the read- out unit and the antennas, were passed through it, and to improve thermal insulation of the oven the remaining aperture was closed with roofmate polystyrene little pieces during tests.

3.3.5 Torque measurement in the Dynamic Set- up

The torque measurement was realized at ambient temperature and performed by acting on the braking system until a relatively stabilized value of perpendicular force applied against the shaft was registered. The rotation speed during the test was given by approximately 150 rpm. The last pulleys assembled to the set- up were included to enhance the transmission of power to the shaft, however the shaft speed was reduced by the same factor. This meant that the maximum speed that could be reached would be ≈375 rpm, far from the range at which, during the tests to evaluate uncertainty, vibration became problematic.
The force values sensed by the load cell were transduced and monitored using the GUI of the program LabView. Data points were extracted at force values comprehended between [0;

2000] N, successively stepped by ≈250 N. The recording process was done using approximately 10 seconds per point of force, to avoid the heating of the braking pad, which would affect the measurements.

Chapter 4

SAW TECHNOLOGY CHARACTERIZATION AND VALIDATION FOR GEARBOX INSTRUMENTATION

A series of tests were performed, with the resolve to characterize the various devices employed in the application at hand. To describe the electrical behaviour of the designed RF coupler antennas, measurements of their S parameters were performed with the resort to a VNA(Vector Network Analyser) Agilent E8361C at the RF laboratory of the Institute of Telecommunications in Aveiro. After studying other topologies advantages/disadvantages, as presented in the previous Chapter, it was decided to implement a large diameter coupler topology, since it was the one that better fit the project requirements.
To characterize the electrical behaviour of the acquired commercial SAW sensors, the S11 response of the sensors was measured in the VNA mentioned before, as presented in figure 2.9.
The relation between temperature and the sensor resonant frequency of the temperature sensors was analysed, in a series of experiments in a temperature chamber ACS Challange 340, with a $2,5m^3$ heating area, located in the second building of the Institute of Telecommunications of Aveiro, employing temperature sensors available within the kit SENSeOR TSE F162 that works in the 433 MHz band.
The behaviour of the strain sensors was also analysed in a series of tests. The objectives were the study of the resonant frequency dependence with respect to temperature, by applying the same method as in the previous case, and its resonant frequency dependence with respect to applied torsional strain in a statical set-up, to acquire a calibration curve to be used in the torque measurements performed in the dynamic set-up.
Tests to determine the effect of speed and temperature in the measurements of both type of sensors were also performed.

Finally, using the dynamic set-up with the modification presented in figure 3.12, torque was measured at ambient temperature.

4.1 Couplers Characterization

In the coupler characterization tests the S11, S21 and S22 parameters were measured in a test bench which allowed a rotation over the 360º. Samples were taken each 5º.
The data obtained was the following:

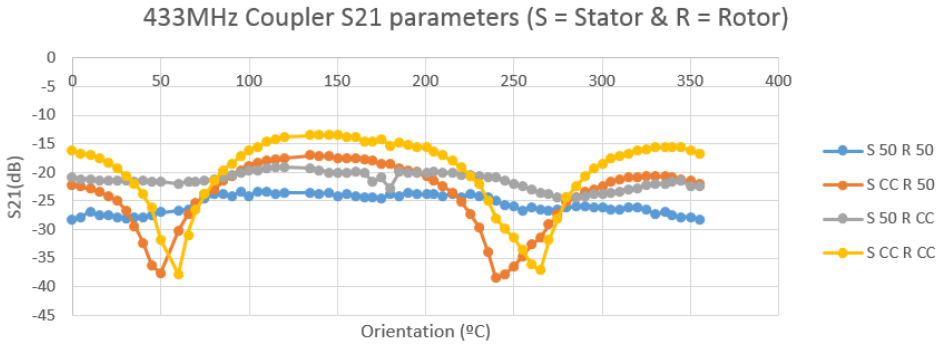

Figure 4.1: 433 MHz coupler S21 parameters measured for each topology

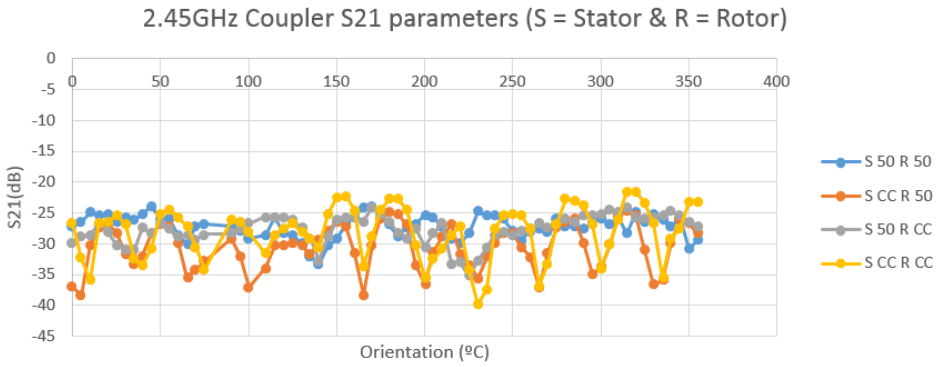

Figure 4.2: 2.45 GHz coupler S21 parameters measured for each topology

It can be easily observed from the 433 MHz coupler measurements graph, that the introduction of a 50 Ω resistor in the Stator's coupler third port, flattens the response for all rotation angles. The termination of the referred port with short- circuit, generates a standing wave pattern with periodic negative peaks in the transmission, which might threaten communication. The results in the 2,45 GHz are not so obvious, since even with a 50 Ω resistor in the stator variable port the response is not so flatten as in the previous frequency and in general transmission is considerably worse, since bigger peak to peak amplitude can be observed.
It is clear that the best topology, includes a 50 Ω resistor termination in the stator. The

use of a 50 Ω resistor termination in the Rotor is around 5 dB worse than a short- circuit termination, without compromising the flatness of the response for all orientations in the 433 MHz case and although in the 2.45 GHz, that is not always the case, generally transmission is also improved, meaning that the topology stator - 50 Ω, Rotor – C.C. is the more suitable.

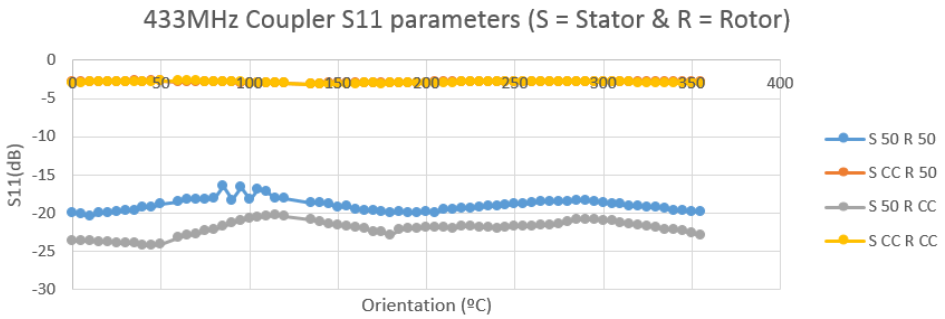

Figure 4.3: 433 MHz coupler S11 parameters measured for each topology

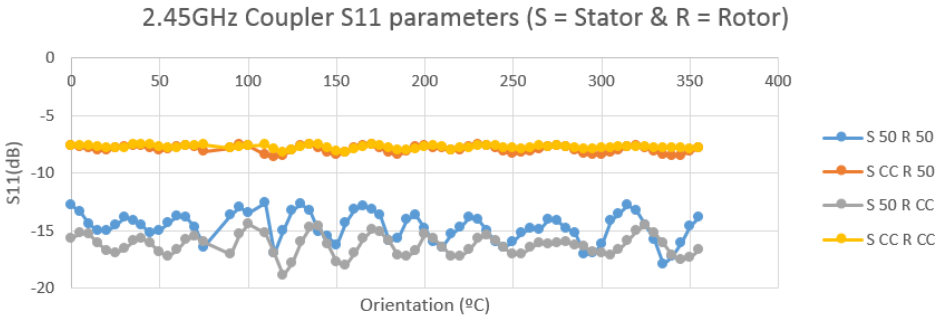

Figure 4.4: 2.45 GHz coupler S11 parameters measured for each topology

As expected, the reflection at the Stator port 1 increases, with the introduction of a matched load in the port 3 termination, however as was concluded before, without the resistor transmition reliability is compromised.

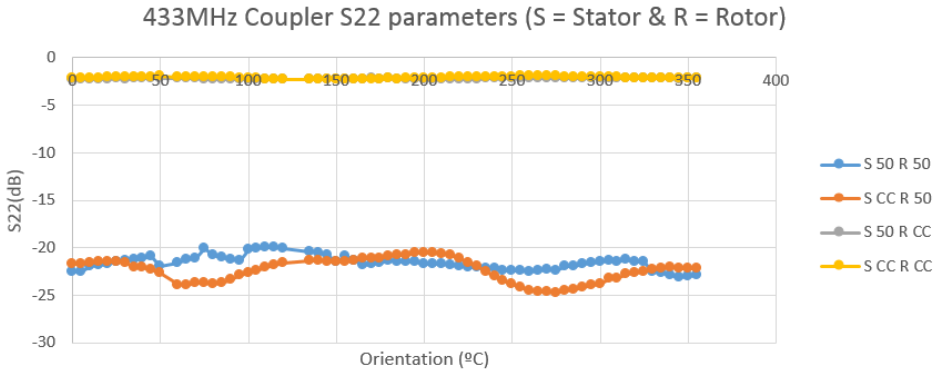

Figure 4.5: 433 MHz coupler S22 parameters measured for each topology

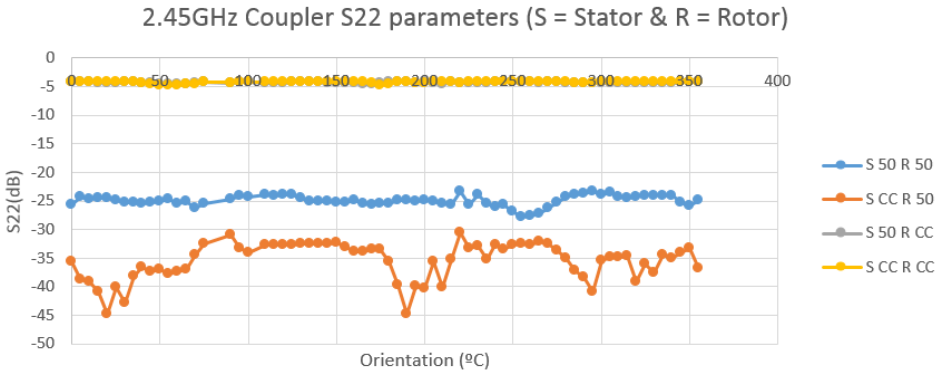

Figure 4.6: 2.45 GHz coupler S22 parameters measured for each topology

As expected, the reflection at the Rotor port 2, where the SAW sensor is connected, increases with the introduction of a matched load in the port 4 termination.

4.2 Temperature Sensors Characterization

The measurements were performed in sets of 4 different scenarios, the first employing measurements with the sensors and the SENSeOR interrogation unit connected to the dipole antenna available within the kit, and the remaining three scenarios using the RF large diameter rotary coupler. Different orientation between the coupler designed for the stator part of the gearbox and the rotor coupler spaced by 120 º were tested.
Regarding the SENSeOR TSE F162 SAW temperature sensor being characterized, it is a double resonator with a registered datasheet resonant frequency at room temperature of 435.9 MHz $\pm$ 0.15 MHz and 436.8 MHz $\pm$ 0.15 MHz, for the first and second resonator respectively. The resonant frequency dependence with respect to temperature, of each resonator, is given

by the following expression:

$$f_{r_i}(T) = f_{r_i}(T_0)(1 + C1_i * (T - T_0) + C2_i * (T - T_0)^2), i = 1, 2. \tag{4.1}$$

where C1 and C2 are the typical first and second order temperature coefficients, of each individual resonator respectively and $T_0 = 25\ ^oC$, given in the datasheet as follows

Table 4.1: First and second order coefficients, of each resonator, as presented in the manufacturer datasheet

	Resonator 1	Resonator 2
C1	4.8 ppm / ^{o}C	- 1.44 ppm / ^{o}C
C2	- 24.6 ppb / $^oC^2$	- 33.1 ppb / $^oC^2$

The fact that the first order TCFS, which are the more significant ones to the determination of the resonant frequency, are of opposite signs improves the resolution of the resonant frequency wrt temperature using a differential measurement, since the absolute value of this coefficients will sum.
The expression that obtained using the differential value between the normalized resonant frequencies of each resonator employed as the output of our measuring system, is the following:

$$y = \frac{f_{r_1}(\Delta T)}{f_{r_1}(T_0)} - \frac{f_{r_2}(\Delta T)}{f_{r_2}(T_0)} \tag{4.2}$$

After some straightforward mathematical deduction the expression that allow us to calculate theoretically the temperature, can be obtained, as a result of the realized measurements, applying the quadratic formula:

$$[C2_1 - C2_2]\,\Delta T^2 + [C2_1 - C2_2]\,\Delta T - \left[\frac{f_{r_1}(\Delta T)}{f_{r_1}(T_0)} - \frac{f_{r_2}(\Delta T)}{f_{r_2}(T_0)}\right] = 0 \tag{4.3}$$

$$ax^2 + bx + c = 0 \tag{4.4}$$

from which we extract the coefficients,

$$a = [C2_1 - C2_2] \tag{4.5}$$

$$b = [C2_1 - C2_2] \tag{4.6}$$

$$c = -\left[\frac{f_{r_1}(\Delta T)}{f_{r_1}(T_0)} - \frac{f_{r_2}(\Delta T)}{f_{r_2}(T_0)}\right] \tag{4.7}$$

The measurements were realized, for temperature points, with intervals comprehended between 0 °C and 80 °C, generally with spacement of 10 °C between successive points. At 25°C a measurement was performed in all scenarios, to utilize as reference when tracing the frequency wrt temperature curve. Figures 4.7, 4.8, 4.9 and 4.10 represent the measurements realized with the SENSeOR 433 MHz interrogation unit and the TSE F162 SAW temperature sensor. The column on the right of the data curves corresponds to the temperatures inferred from the measured resonance values, calculated from expression 4.3, using the theoretical coefficients given in the datasheets.

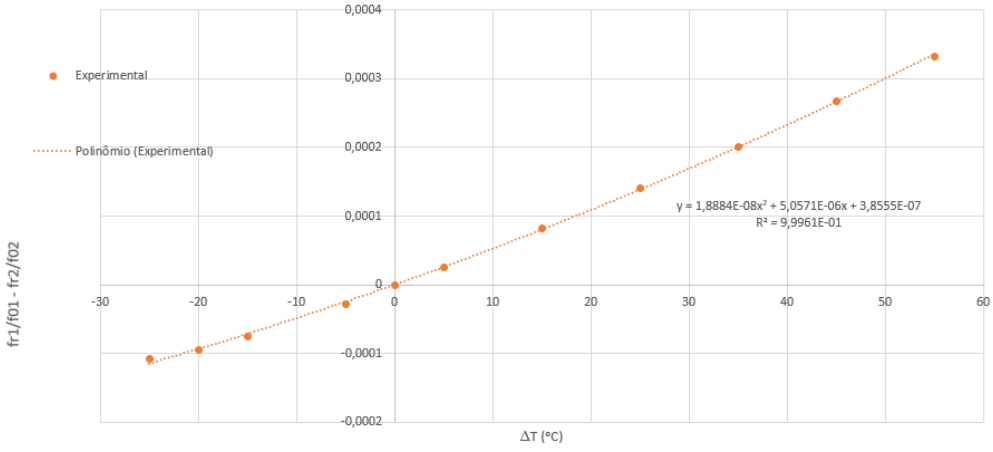

T
7,07494263
9,3853468
12,7462789
20,3730314
25
29,0207186
38,1438767
47,1140863
56,171963
65,8557329
75,2392634

Figure 4.7: Results of Δf vs Temperature obtained for measurements with the 433MHz kit a dipole antenna (on the left) and the theoretical temperatures calculated from measurements at each point(on the right)

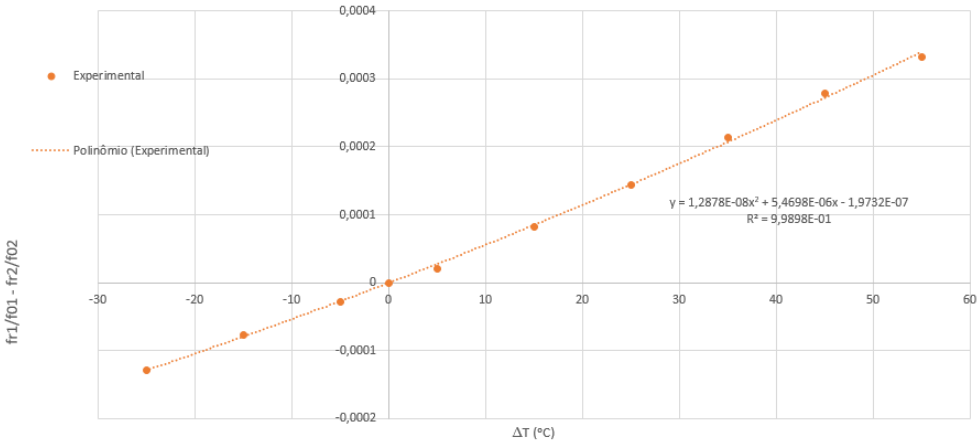

T
3,720902234
12,43198365
20,56124838
25
28,22138293
38,09013381
47,54294791
58,03920819
67,48648798
75,12913337

Figure 4.8: Results of Δf vs Temperature obtained for measurements with the 433MHz kit, with rotor and stator couplers with an orientation of 0 º beetween them (on the left) and the theoretical temperatures calculated from measurements at each point(on the right)

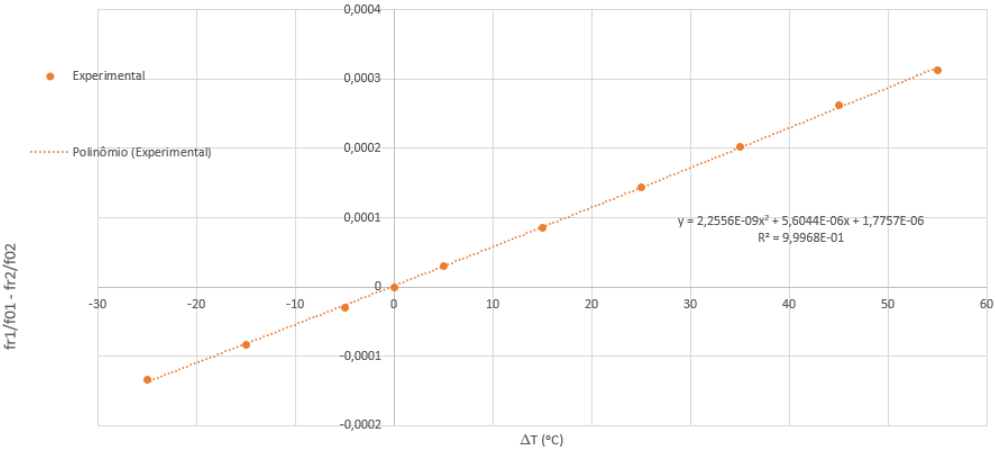

T
2,77500763
11,2394271
20,28118
25
29,9829815
38,5209197
47,5944907
56,3777855
65,0858736
72,3758948

Figure 4.9: Results of Δf vs Temperature obtained for measurements with the 433MHz kit, with rotor and stator couplers with an orientation of 120 º beetween them (on the left) and the theoretical temperatures calculated from measurements at each point(on the right)

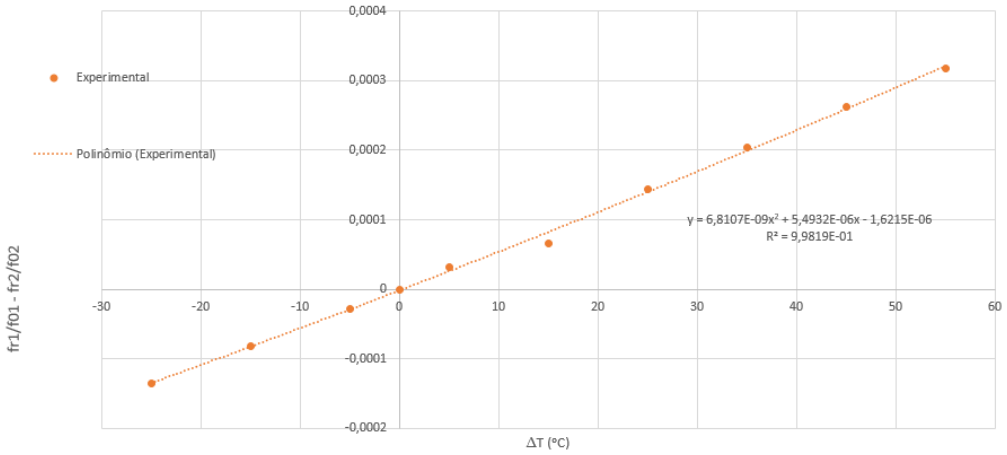

T
2,48755
11,5025
20,4667
25
30,0384
35,4897
47,5764
56,4611
65,1781
73,0205

Figure 4.10: Results of Δf_n vs Temperature obtained for measurements with the 433MHz kit, with rotor and stator couplers with na orientation of 240 ^{o} beetween them (on the left) and the theoretical temperatures calculated from measurements at each point(on the right)

From the graphs above, analysing the table values at the right of the image, it is possible to conclude that: the temperature calculated fitting the resonant frequencies extracted on expression 4.3 using the TCFs given by the manufacturer are expected; From expression present on the calibration curves of figures 4.8, 4.9, 4.10 it is possible to extract the calibration TCF of the TSF162 SAW sensors. The calibration curve has the form

$$y = a\Delta T^2 + b\Delta T \tag{4.8}$$

The calibration coefficients a and b are obtained by calculating the mean of the values obtained in the tests employing RF Couplers. The values obtained were the following:

$$a = 7,3112 * 10^{-9} \tag{4.9}$$

$$b = 5,5225 * 10^{-6} \tag{4.10}$$

The deviation in the theoretically calculated temperature can be expained by the fact that the calibration procedures here presented are naturally not similar to the ones employed by the manufacturer at the time the datasheet parameters were obtained.
At last, the fact that the temperature sensor is mounted in a PCB as indicated in the datasheet, which naturally constitutes a thermal resistor, might be a factor that contributes with error in the measurement.

4.3 Strain Sensors Characterization

The strain gages employed were the SENSeOR single resonators SEE E015 and SEE E016. The resonant frequencies at room temperature, indicated in the manufacturer datasheet are

respectively 433.97 MHz ± 0.15 MHz and 432.59 MHz ± 0.15 MHz.
The configuration employed was a Half- Bridge [39], characterized by the fixation of the strain gages 90 ^{o} from each other, in a position of 45 ^{o} each, in respect to the shaft axis, as exemplified in the figure 4.11.

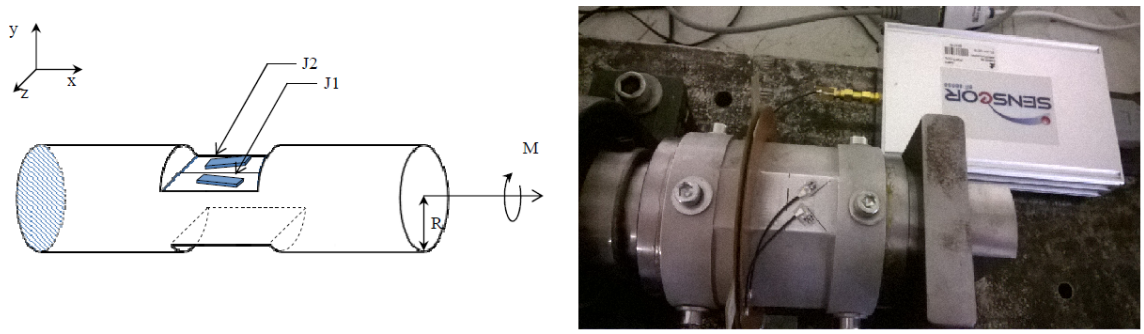

Figure 4.11: Half- Bridge configuration for Torque measurement, as in the SENSeOR technical manual (left) [39]. Static set- up assembled in a Half- Bridge configuration (right).

According to the SENSeOR technical manual previously referred [39], a value of torque measured can be calculated, based on the expression

$$M = \frac{2JG\epsilon}{R} \tag{4.11}$$

where, G is the shear modulus, which in the case of aluminium is tabulated as 25.5 GPa [40], ϵ the measured strain, R is the radius of the rod under test and J is the Quadratic Moment

$$J = \frac{\pi R^4}{2} \tag{4.12}$$

From the measurement of strain obtained by the sensor, values of torque applied to the Load Cell, can be extrapolated. The sensors used were the strain gages from SENSeOR SSE E015 and SSE E016, which consist in SAWRs to be used in pairs.
The resonant frequency of a strain sensor, wrt strain is given as [39]

$$f_r(T) = f_0(25^oC)[1 + C1 * (T - 25^oC) + C2 * (T - 25^oC)^2 + S_g\epsilon] \tag{4.13}$$

where $f_0(25^oC)$ is resonant frequency at 25^{o}, without strain applied, S_g is the gage factor of the strain sensors, which is obtained from the calibration curve slope. ϵ is the strain along the gage axis, finally, C1 and C2 are the typical first and second order temperature coefficients of each individual resonator respectively, given in the datasheet as follows

Table 4.2: First and second order coefficients, of each sensor, as presented in the strain gage manufacturer datasheet

	Sensor E015	Sensor E016
C1	0.9 ppm / ^oC	0.9 ppm / ^oC
C2	- 24.8 ppb / $^oC^2$	- 24.8 ppb / $^oC^2$

The SAWRs are use in pairs because they were manufactured to have equal TCFs, so that the use of a differential normalized output would cancel the temperature dependence factors. In practice due to differences between the sensors and imperfection in the sensor fixation, a quadratic variation of the differential output wrt to temperature is verified.
Regarding the measurement of strain ϵ in the Load Cell, accordingly to what is specified in the *SENSeOR "Strain gages measurement configurations"* manual, the theoretical output of the interrogation unit in a conveniently prepared set- up in a Half- Bridge configuration, relates the differential value between the normalized resonant frequencies and the Gage Factor S_g:

$$\frac{f_{15}(\Delta T, \epsilon)}{f_{15}(T_0, 0)} - \frac{f_{16}(\Delta T, \epsilon)}{f_{16}(T_0, 0)} = 2S_g\epsilon \tag{4.14}$$

The objective of the calibration is to obtain a curve better representing the sensors response due to the conditions of the test, given that the conditions under which the sensors were evaluated by the manufacturer to reach the given TCFs and reference frequencies are naturally different than the ones at hand.
By acquiring the resonant frequencies for some applied torque values and using polynomial fit in the relation between these points, one obtains the Gage Factor by relation with the curve slope.
The variation of the conditions in the mechanical set- up in rotation mode relatively to static condition shouldn't be significant so dynamic calibration may not be necessary.
Calibration curves for both the sensors dependence to temperature and strain were acquired.

4.3.1 Calibration of the Strain Gages for Torque Measurement

The calibration curves obtained in the experiment of figure 3.16(a) and 3.16(b) are observed in figure 4.12 and 4.13 respectively:

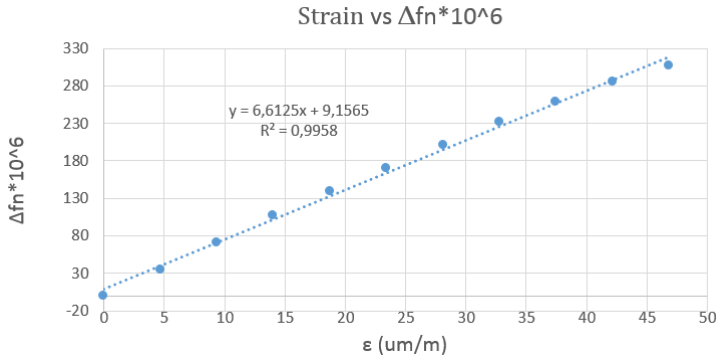

M(experimental)	M(theoretical)	ε(experimental)	ε(theoretical)
0,0	0,0	0,0	0,0
19,0	21,2	4,7	5,2
38,0	43,3	9,4	10,7
57,0	65,8	14,0	16,2
76,0	85,6	18,7	21,1
95,1	104,5	23,4	25,8
114,2	123,5	28,2	30,4
133,0	141,7	32,8	34,9
152,1	158,3	37,5	39,0
171,2	175,5	42,2	43,2
190,1	188,1	46,9	46,3

Figure 4.12: Calibration line obtained (downward vertical direction), with info regarding frequency, with respect to the measured strain

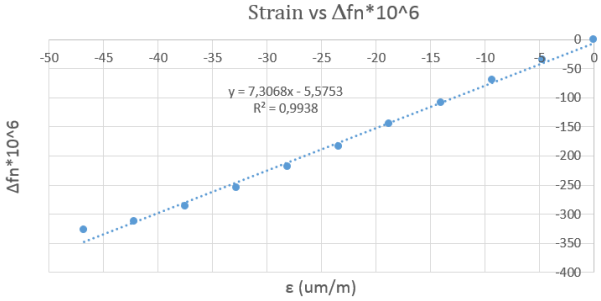

M(experimental)	M(theoretical)	ε(experimental)	ε(theoretical)
0,0	0,0	0,0	0,0
-19,0	-19,2	-4,7	-4,7
-38,0	-39,1	-9,4	-9,6
-57,0	-60,4	-14,0	-14,9
-76,1	-80,4	-18,8	-19,8
-95,1	-102,3	-23,4	-25,2
-114,0	-121,6	-28,1	-30,0
-133,0	-141,7	-32,8	-34,9
-152,0	-159,2	-37,5	-39,2
-171,0	-174,0	-42,1	-42,9
-190,0	-181,3	-46,8	-44,7

Figure 4.13: Calibration line obtained (upward vertical direction), with info regarding frequency wrt the measured strain

The calibration curve obtained has the form

$$g(\epsilon) = 2S_g\epsilon \tag{4.15}$$

Torque measurement in the dynamic set- up was only performed with strain applied in the cell, in the same direction of the experiment 3.16(a).
The Gage Factor extracted from figure 4.12 is

$$S_g = 3,3063 \tag{4.16}$$

The observable difference in the lines obtained in figure 4.12 and 4.13 and the different offset in the frequencies obtained, can be explained by the hysteresis associated to the Testing Machine itself, when applying Forces in opposite directions or the backlash of the mechanical set- up could also have effect between results.

4.3.2 Calibration of the Strain Gages in Temperature

The study of the utilized SAW strain gages was continued, by evaluating their behaviour when these are subjected to temperature variation.

From the data obtained in the practical experiment, the effect of temperature on the Δf_n, corresponding to the normalized difference between the resonant frequencies of both resonators, was calculated in the following curve:

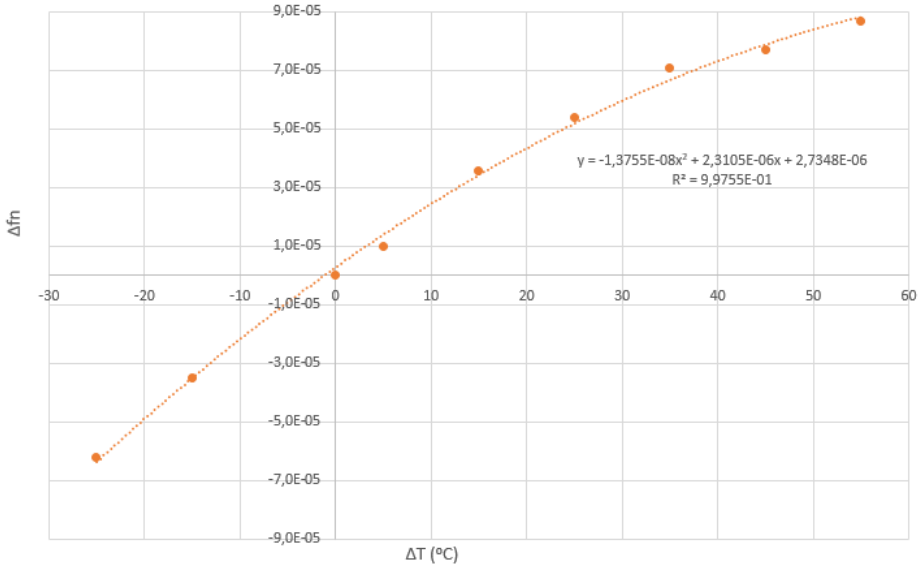

Figure 4.14: Normalized difference between the resonant frequencies of SAW strain gages SSE E015 and SSE E016 wrt temperature

As mentioned before, the normalized differential measurement didn't cancel the temperature effect on the measurement since the curve obtained behaves as a second order equation. The curve fitting performed in the previous image gives us the first and second order coefficients of the calibration curve of the strain gages in temperature, to be used for temperature compensation in the torque measurements. The calibration curve obtained has the form

$$f(\Delta T) = a\Delta T^2 + b\Delta T \tag{4.17}$$

The calibration coefficients a and b obtained were the following:

$$a = -1,3755 * 10^{-8} \tag{4.18}$$

$$b = 2,3105 * 10^{-6} \tag{4.19}$$

4.4 SAW Sensors Uncertainty Tests

First an analysis on the propagation error intrinsic to the frequencies extraction is made. The uncertainty in the temperature measurement in static conditions (the only source of error is in the resonant frequency estimation, assuming that the RF coupler has an ideal behaviour)

can be theoretically determined by applying the formula of the Propagation of Errors to the expression 4.21.
The system output dependence wrt to temperature is given by an expression with the form

$$\Delta f_n(\Delta T) = \frac{f1}{f0_1} - \frac{f2}{f0_2} = a\Delta T^2 + b\Delta T \tag{4.20}$$

where Δf_n is the normalized difference between the resonant frequencies, f1 and f2 are the estimated resonant frequencies and $f0_1$ and $f0_2$ are the reference value at 25 ^{o}C. From the previous formula we extract that,

$$\Delta T = \frac{-b + \sqrt{b^2 + 4a\Delta f_n}}{2a} \tag{4.21}$$

The propagation error of the previous formula is given as

$$(\Delta T(\Delta f_n))^2 = \sum_{i=1}^{n} \frac{\delta \Delta T}{\delta \Delta f_n} |\Delta f_n| \tag{4.22}$$

The contribution on the temperature error due to the system output is given as

$$\frac{\delta \Delta T}{\delta \Delta f_n} = \frac{1}{\sqrt{b^2 + 4a\Delta f_n}} \tag{4.23}$$

The absolute error expression of the system output is the following:

$$|\Delta f_n|^2 = |\Delta f1|^2 \left| \frac{\delta \Delta f_n}{\delta f1} \right|^2 + |\Delta f2|^2 \left| \frac{\delta \Delta f_n}{\delta f2} \right|^2 \tag{4.24}$$

The absolute error of the system output is the following

$$|\Delta f_n| = |\Delta f_r| \sqrt{\frac{f2^2 + f1^2}{f2f1}} \tag{4.25}$$

where f_r is the resonance of the sensor or resonator in cause. $|\Delta f_r|$ is given by the interrogation window divided by the number of window points selected. The final expression for the error propagation of the temperature measurement follows:

$$|\Delta T| = |\Delta f_r| \sqrt{\frac{f2^2 + f1^2}{f2f1}} \frac{1}{\sqrt{b^2 + 4a|\Delta f_n|}} \tag{4.26}$$

On the other hand, the determination of the torque error is obtained by applying the propagation of errors in the following expression:

$$M = -\frac{\pi R^3 G}{2S_g} \left| a\Delta T^2 + b\Delta T + \frac{f2}{f0_2} - \frac{f1}{f0_1} \right| \tag{4.27}$$

The partial contributions to the error are given by

$$\left|\frac{\delta M}{\delta fi}\right| = \frac{\pi R^3 G}{2 S_g f0_i}, i = 1, 2. \tag{4.28}$$

$$\left|\frac{\delta M}{\delta \Delta T}\right| = \frac{\pi R^3 G}{2 S_g}[2a\Delta T + b] \tag{4.29}$$

The final expression is obtained by simple deduction as follows

$$|M| = \frac{\pi R^3 G}{2 S_g}\left||f_r|^2 \frac{f0_2^2 + f0_1^2}{f0_1^2 f0_2^2} + |\Delta T|^2 (2a\Delta T + b)\right| \tag{4.30}$$

This deduced propagation errors are considerably inferior to the systematic and random errors present in the system during rotation. The rotation errors associated with speed and temperature are analysed in the subsequent subsections.

4.4.1 Temperature Sensors Experimental Uncertainty

The SAW sensors uncertainty evaluation was performed in tests at three different temperature set points of 25 °C, 47.5 °C, 60 °C, at different rotation speed values. In figure 4.15 the standard deviation of the registered differential temperature values of frequency is presented.

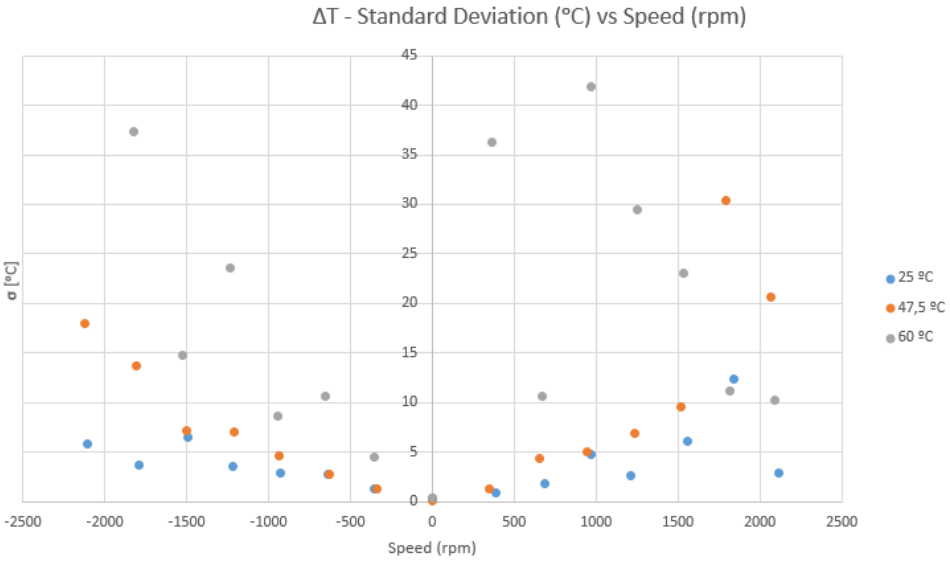

Figure 4.15: Standard deviation of the temperature sensors measured ΔT wrt speed and temperature

In figure 4.16 the calculated mean values of ΔT at each data set, is presented.

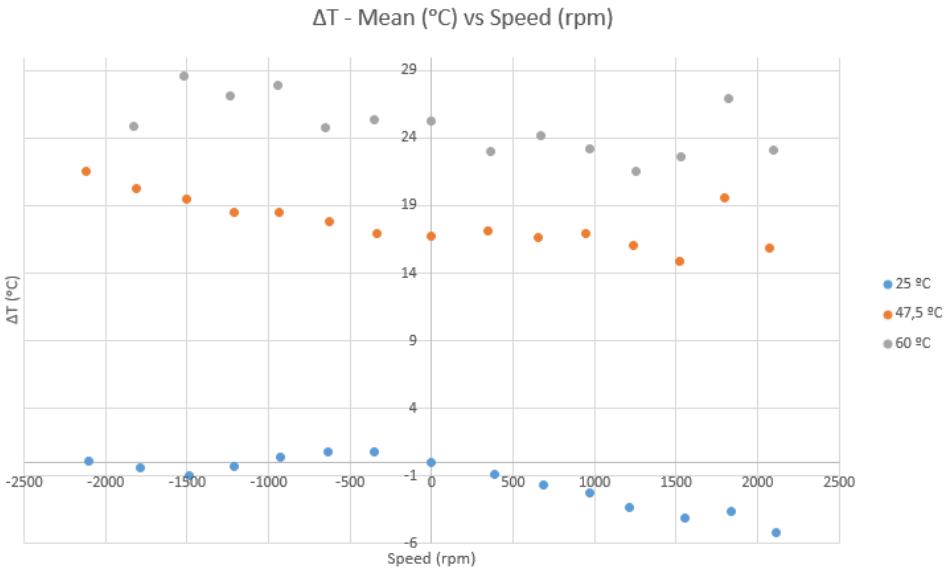

Figure 4.16: Standard deviation of the temperature sensors mean measured values of ΔT wrt speed and temperature

Relatively to the temperature sensors results, the standard deviation and the calculated mean values at ambient temperature are expectable for the most of the speed points. However, at 47.5º and 60º the results considerably lack precision, particularly in the last case. In the 60º set points with standard deviation over 30º, bad adaptation was detected.

4.4.2 Strain Gages Experimental Uncertainty

In figure 4.17 the standard deviation of the differential registered values of frequency is presented.

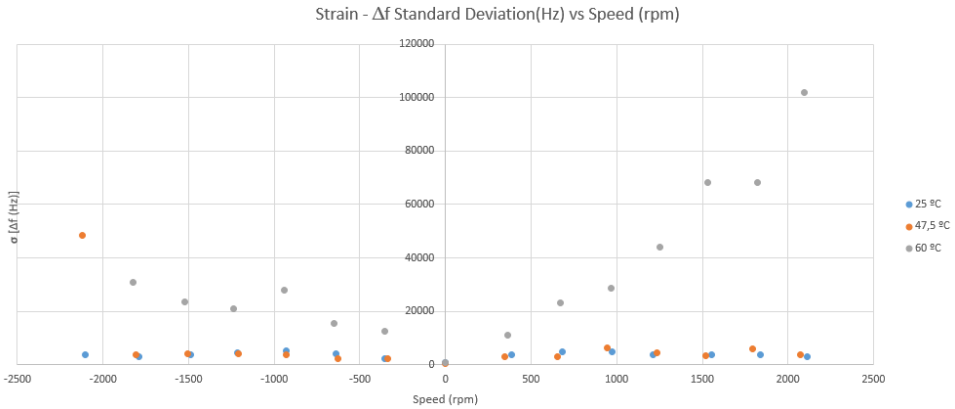

Figure 4.17: Difference between the strain sensors Δf measured wrt speed and temperature when compared with results obtained in static conditions

After analysis of the frequencies extracted in the 60º data set, it was concluded that one of the sensors was badly connected, so that data was excluded. It is more notorious in the rotative positive direction, that the standard variation at 60º rises enormously when compared with the previous cases. In fact, one of the issues that emerged was the instability caused by the centrifugal forces caused in the U-FL cables with length superior to 5 mm due to speed. The use of small cables (for example 5 mm) or strategies to improve its stability such us, surrounding them with a weightless teflon tape might be crucial to minimize the uncertainty of the data.

Figure 4.18 gives the standard deviation of the calculated torque at each data set.

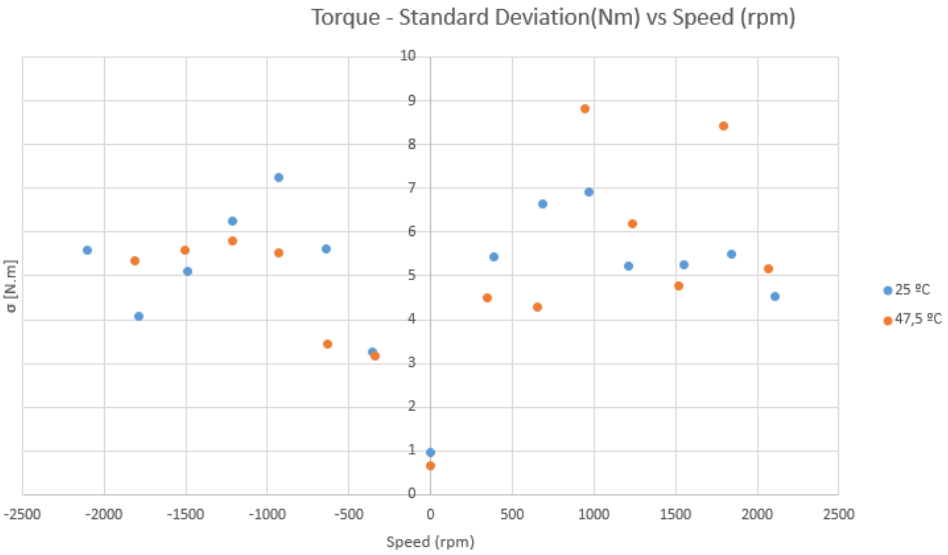

Figure 4.18: Standard deviation of the sensors measured torque wrt speed and temperature

Figure 4.19 gives the calculated mean values of torque at each data set.

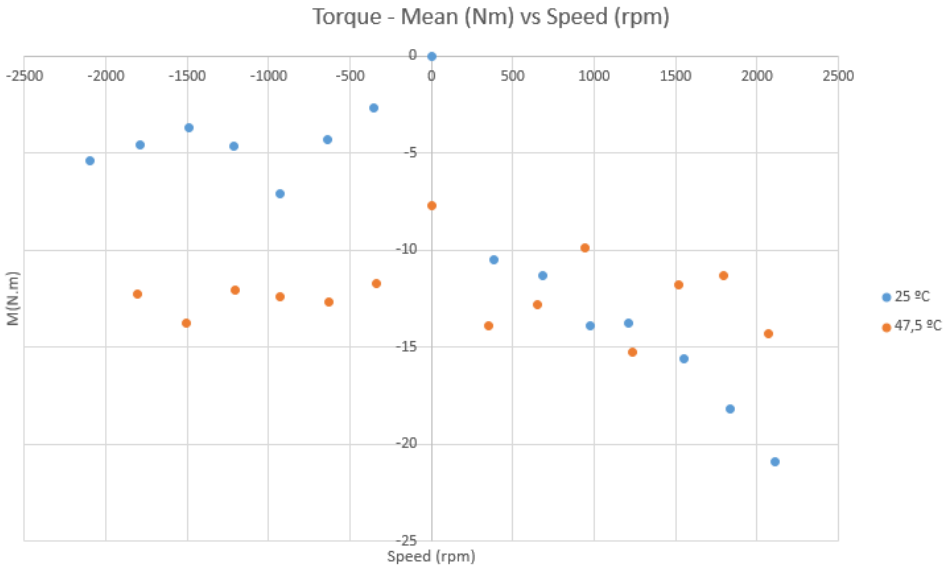

Figure 4.19: Standard deviation of the sensors mean measured values of Torque wrt speed and temperature

It is clear that the standard deviation with rotation significantly increases, however not unexpectedly. At ambient temperature the calculated mean values in the positive direction of rotation significantly deviate from the proximity of zero and almost linearly increase with speed. In opposite direction it is more stable around -5 Nm. The deviation from zero at 45º increases but the results are more stable between -10 and -15 Nm at rotation. The last point and the fact that in rest a mean value of approximately -7.5 Nm is found, indicates that the error in the calculations caused by the temperature effect on the sensors is considerably high. The deviation of the results in rotation relatively to the registered values at rest indicate that the set- up imperfections have an effect on the measurements that cannot be neglected.

4.4.3 Uncertainty Tests General Remarks

From the graphs presented in the two previous subsections it is possible to generally conclude that as speed and temperature increase the standard deviation of the measurements tends to increase too. The faster the shaft rotates, the more enhanced tend to be the intrinsic vibrations associated to this rotation. However, this behaviour is not linear, since mechanical resonance conditions might happen not necessarily at top speed values.
On the other hand the higher temperature gets, the more significant becomes the error caused by the variation of the sensors temperature calibration due to the RF Coupler orientation. The error due to the difference between the temperature measured by the thermocoupler and the real temperature in the metal of the load cell also tends to increase, since temperature stabilization becomes more difficult.
Standard deviation of the extracted mean values generally decreases after a considerable recording time, meaning that limiting properly the maximum standard deviation in a data

extraction cycle and averaging a relevant quantity of data before calculating a measurement value, might significantly reduce error caused by the dispersion in the data, due to speed and temperature.

4.5 Torque Measurement

The torque measured is given by an expression with the form

$$\frac{f_{15}(\Delta T, \epsilon)}{f_{15}(T_0, 0)} - \frac{f_{16}(\Delta T, \epsilon)}{f_{16}(T_0, 0)} = \Delta f_n = f(\Delta T) + g(\epsilon) \tag{4.31}$$

Deducing the previous formula strain can be calculated as

$$\epsilon = \frac{\Delta f_n - f(\Delta T)}{2S_g} \tag{4.32}$$

Only one experimental set of torque data was extracted due problems with the load cell verified after the experiment being presented and to time constraints.
The data obtained from the measurement is presented in figure 4.20:

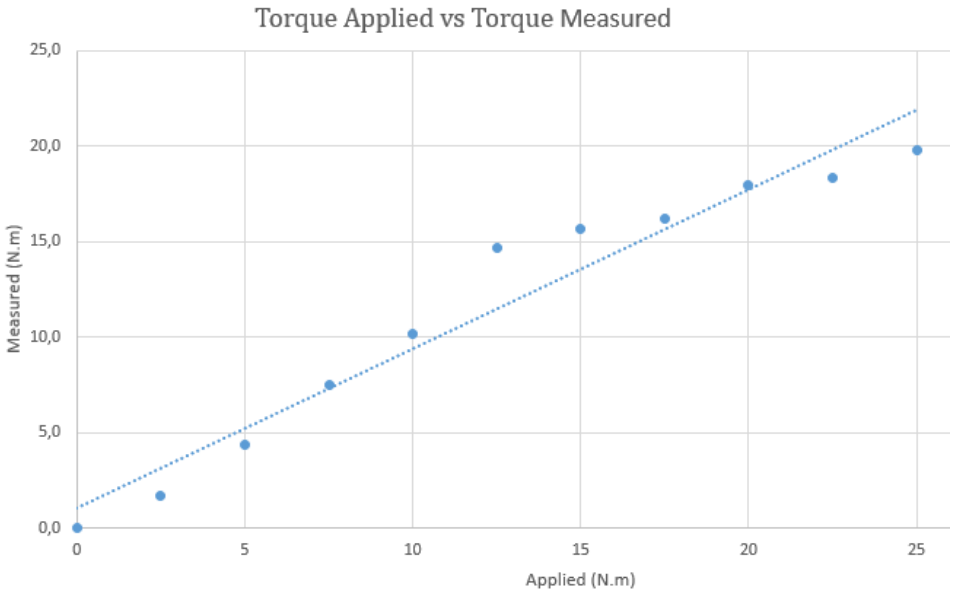

Figure 4.20: Comparison between the applied values and the ones measured using the SAW sensors

From analysis of the torque values calculated in comparison with the torque actually being applied to the cell (figure 4.20), it is observable that the measured value are not far from those expected. A source of slight error is the fact that the reference frequency of each sensor $f0_i$ used were the ones obtained for F = 0 N and the test was performed at ambient temperature, but not exactly 25 °C, this value would be comprehended somewhere between [20; 25] °C. The

shaft bending due to rotation sensed by the strain gages and that is not compensated, even at slow speed might be a possible source of slight error. Major sources of error, particularly as the force by which the braking pad is pressed against the shaft circular section increases, might caused by flexion and compression forces generated in the load cell, due to the rotative shaft misalignment. In fact, the slight accommodation of the shaft to a different position and consequent misalignment, when the higher values of force F were applied, was visible by eye and helps explaining the more significant difference between measured and applied torque in the last data points extracted.

Given that the data is reduced and that, to validate the use of this sensors for torque measurement it would be needed to test them at higher temperatures, higher speed and in a broader range of torque.

Chapter 5

CONCLUSIONS

Finally, let's proceed to the general conclusions and establishment of improvements and future work that could be made to continue the one that was presented in this document.
First, the non-existence of a technology mature enough for direct real- time monitoring of the critical rotative components inside a power reduction gearbox, as far as what is available to the public, opens possibility to further research the present technology with the objective of establishing it as viable for this scenario.
Relatively to the sensors used, the temperature sensor was not the most indicated since its U-FL connection to the coupler was unstable and it was mounted on a PCB wafer, which constitutes a thermal resistance. Using a solution that is not encapsulated and not mounted on a PCB, more similar to the strain gages which are glued to the shaft, could improve the sensor thermal sensitivity.
Two issues surface regarding the adequacy of the strain gages. The first, might be in the epoxy paste used to fix the sensor to the shaft. During the test campaign it was verified in successive experiments that the offset measured had differed between tests, without any modification of the set- ups. To avoid that this issue affected the measurements, test sets of the same experiments were always performed in a row. The offset difference could not simply be explained by the accommodation of the mechanical parts of the set- up because sometimes this variation was significant. Usually after periods of intense test (high values of torque applied or high speed and temperature). Its main causes might be due to some kind of memory effect or hysteresis on the adhesive epoxy layer [41, 42]. This issue deserves a special attention and research to better determine its actual influence on the measurements, since there is not much information about it. The use of paste for strain gages not completely inside the recommendations can also cause the sensors to unstick from the shaft or to be affected in the measurements. The second issue previously referred concerns the U-FL cables and connectors used. It is necessary considerable finesse to handle the sensors, since these are easily damageable. The U-FL connectors are in some sensors are welded to the sensor electrode, meaning they could easily damage the sensor, by simply not properly disconnecting the U-FL cable. During rotation, when the accommodation of the cables was not tight enough, situations in

which due to the centrifugal forces the cables were removed were common. This last point, beyond being risky to the sensor integrity represents another possible source of error since, this same pushing force in the connector might cause variation of the material condition.
In the RF Couplers characterization the test bench itself presented a small vulnerability, in which the tension force of the SMA cable made difficult to maintain the rotor and stator coupler perfectly parallel, but results have gone according to the theoretically expected. The application of the couplers during the tests was successful however, it was difficult to establish perfectly constant unaffected communication at all 360^{o} of rotation since slight deviations in the parallelism between the coupler rings could in some orientations cause signal saturation or signal loss. Thereby, the design of a RF Coupler as insensitive as possible to the deviations in the distance between the rings, small angular variation of the measured resonant frequency and low insertion loss could significantly improve the quality of the data extracted. This factor becomes clearly relevant when vibration in the shaft is significant. It was also detected significant difference in the measured second order temperature coefficients of the sensors at different coupler orientation which might introduce significant error in the temperature measurements.
Regarding the static set- up fabricated and the calibration test performed in it, the two calibration curves for torque measurement extracted were slightly different. In the experiment presented in figure 3.16(a) the Universal Test Machine applied force directly into the moveable arm while at the experiment presented in figure 3.16(b) the perpendicular force applied was applied in the upward direction by connecting the set- up moveable arm to the arm of the test machine using a cable. That difference in procedure is the main cause to the difference in the curve, given that the backlash of the test set- up and the backlash associated to the accommodation of the cable to the tension force applied affect the result. It was also verifiable during the procedure that, there is also some hysteresis associated to the Testing Machine itself, when applying forces in opposite directions. So, using more identical procedures of calibration for torque measurements would be recommended if torque is to be measured applying rotation in both directions.
During the test campaign at some point there was the need to change from strain gages SSE E017 to SSE E016, due to damage of the first. This beyond the natural delay caused by the de-assemble, gages fixation and new assemble of the set- ups, caused considerable delay because the firmware of the WRD005 read- out unit was not prepared to extract information from the new sensors operation band, until it was updated. So it is important to guarantee compatibility between the acquired sensors and the read- out unit to avoid unnecessary delays.
On the other hand, the dynamic set- up main difficulties were: the fixation of the coupler rings in a perfectly parallel position (this issue would get worse with use since, the metallic L-shaped piece fixing the stator coupler, due to vibration and forces felt during the experiments would gradually deviate from the initial position). A more robust method for the fixation of the couplers is recommended; The lack of temperature stability in the oven was an issue if torque measurements at high temperatures were to be performed and using the thermocoupler as reference for the measurements was also not an ideal solution since it didn't extract the exact

temperature in the metal; The perfect alignment of the shafts connected by the load cell might be challenging and important to the accuracy of the measurements. A non-aligned set- up beyond having more intrinsic vibration, applies flexion forces in the load cell that affect the measurements and that in more extreme cases might deform the load cell.
The uncertainty associated with speed and temperature is significant. The error in the determination of the frequencies under rotation is dependent on the mechanical behaviour of the set-ups at certain speed and temperature values and on the coupler orientation at the exact extraction moment. In the case of the strain gages it is also dependent on the material conditions change due to the connectors being centrifugally pushed by the cables. Error can be slightly diminished by the time taken to extract valid frequencies and averaging and by controlling the maximum standard deviation allowed in a interrogation cycle.
The dynamic set- up would need further improvements to perform proper torque measurements. The used AC motor lacks power to embrace the desired range of torque so it should be substituted by one that would meet the requirements. The brake pad was not perfectly aligned with the shaft and therefore, did not apply evenly friction in the contact area and the friction coefficient used was not properly estimated, so a standard value was used. This issues imply a slight error in the estimation of torque.
Finally, regarding the objectives proposed: the calibration of the strain sensors for torque measurements at ambient temperature was successful; It was proved that it is possible to measure temperature and torque in rotation using this sensors and interrogation unit; The effect of speed and temperature in the measurements was studied, however experimenting in one more temperature data point closer to the range superior limit would improve the conclusions obtained; Regarding torque measurement, the data extracted is reduced, so in order to obtain validation it would be needed to test the SAW sensors at higher temperatures, higher speed and in a broader range of torque.
As a last note, the templates used to analyse the data relative to the work done is provided in the CD delivered to the Aveiro University together with this dissertation.

5.1 Future Work

The future work to be done to improve the study realized in this work consist is proposed in the following topics:
Fabricate or buy new sensors without connectors. A possible solution would be one in which the sensors were fixed in the load cell and connected to an auxiliary PCB via wire bonding.
Improve the dynamic set-up. First, study of the mechanical resonance of the dynamic set- up and its effects and construct a new set- up having the previous conclusions in mind. Next, develop a more stable form to fixate the stator coupler and fixate the two couplers in parallel in more precise way. Fabricate of improved RF Couplers, using a substrate with lower insertion loss. This would allow increasing the distance between the couplers which would improve communication link stability. Then, performing an alignment as precise as possible

of the shafts connected to the load cell and of the braking system. A solution without bearing and metallic support pieces, using a single mechanical part machined in order to precisely align the whole shaft is a possibility. Limit the number of screws in the load cell is also recommended. To increase the applied torque, substitution of the rotation shaft by one with higher radius and improvement of the power transmission system is also recommended. After that, improve the braking system and perform a test to acquire the real value of the friction coefficient of the brake friction material used. Substitute of the oven by a model that better stabilizes temperature and use a solution able to measure temperature directly in the load cell metal. Finally, substitute the AC motor by another model able to provide the power needed to measure torque in the interest range.

Perform calibration tests in both directions using more similar procedures. Perform more tests to better evaluate the effect of the couplers orientation in temperature calibration of the sensors and decrease its effect. Perform further tests to more precisely learn the uncertainty caused by rotation speed and temperature in the sensors, using the improved set- up and sensor solutions. Research on the epoxy paste effect on the measurements. After the referred improvements are done perform torque measurements using full-bridge configuration at higher speed and temperatures, and in a broader range to achieve validation to determine the validation or not of the technology for gearbox instrumentation.

Bibliography

[1] A. Lonsdale and B. Lonsdale, "Method and apparatus for measuring strain," Dec. 17 1996. US Patent 5 585 571.

[2] V. Kalinin, "Wireless physical SAW sensors for automotive applications," *IEEE International Ultrasonics Symposium, IUS*, pp. 212–221, 2011.

[3] L. Reindl, F. Schmidt, O. Sczesny, and V. Mágori, "Remote Sensing of Physical Parameters By Means of Passive Surface Acoustic Wave Devices," *IEEE 1994 Ultrasonic Symposium*, pp. 589–592, 1994.

[4] L. Reindl, G. Scholl, T. Ostertag, A. Pohl, and R. Weigel, "Wireless remote identification and sensing with SAW devices," *Proc. IEEE*, pp. 83–96, 1998.

[5] L. Reindl, "Theory and application of passive saw radio transponders as sensors," *IEEE Transactions on Ultrasonics, Ferroelectrics, and Frequency Control*, vol. 45, no. 5, pp. 1281–1292, 1998.

[6] D. Macário, "Utilização de Dispositivos de Onda Superficial Como Sensores e Identificadores," Master's thesis, Universidade de Aveiro, Aveiro, 2007.

[7] V. Kalinin, A. Leigh, A. Stopps, and E. Artigao, "Resonant SAW torque sensor for wind turbines," *2013 Joint European Frequency and Time Forum and International Frequency Control Symposium, EFTF/IFC 2013*, pp. 462–465, 2013.

[8] S. Ackert, "Basics of Aircraft Maintenance Reserve Development and Management," 2012.

[9] K. A. Jason and K. S. Aryan, "A Survey of Health and Usage Monitoring System in Contemporary Aircraft," no. 9, pp. 34–41, 2013.

[10] W. Hong, S. Wang, M. Tomovic, L. Han, and J. Shi, "Radial inductive debris detection sensor and performance analysis," *Measurement Science and Technology*, vol. 24, no. 12, p. 125103, 2013.

[11] K. Cassidy, "Qualifying an On-Line Diagnostic and Prognostic Sensor for Fixed and Rotary Wing Bearings and Gears," no. March, 2008.

[12] L. Overmeyer, J. Duesing, O. Suttmann, and U. Stute, "Laser patterning of thin film sensors on 3-d surfaces," *{CIRP} Annals - Manufacturing Technology*, vol. 61, no. 1, pp. 215 – 218, 2012.

[13] Y. Oniwa, T. Miyoshi, K. Fujita, A. Yoneda, and Y. Shimizu, "Magnetostrictive torque sensor and electric steering system," May 10 2011. US Patent 7,938,026.

[14] Y. Wang, Y. Jia, Q. Chen, and Y. Wang, "A passive wireless temperature sensor for harsh environment applications," *Sensors*, vol. 8, no. 12, p. 7982, 2008.

[15] "Rayleigh wave." `https://en.wikipedia.org/wiki/Rayleigh_wave`. Accessed: 2016-02-25.

[16] D. Branch, "Surface-acoustic-wave devices," *AccessScience, McGraw-Hill Education*, 2014.

[17] C. Campbell, *Surface Acoustic Wave Devices for Mobile and Wireless Communications*. Academic Press, 1st ed., June 15 1998.

[18] R. M. White, "Surface Elastic Waves," *Proceedings of the IEEE*, vol. 58, no. 8, pp. 1238–1276, 1970.

[19] A. Polh, "A review of wireless SAW sensors.," *IEEE transactions on ultrasonics, ferroelectrics, and frequency control*, vol. 47, no. 2, pp. 317–332, 2000.

[20] L. Alves, J. Mendes, and A. Barata, "2.2 - Concept Design," tech. rep., Universidade de Aveiro, Departmento de Eletrónica, Telecomunicações e Informática, 2016.

[21] R. White and F. Voltmer, "Direct piezoelectric coupling to surface elastic waves," *Applied Physics Letters*, vol. 7, no. 12, pp. 314–316, 1965.

[22] R. Tancrell, M. Schulz, H. Barrett, L. Davis, and M. Holland, "Dispersive delay lines using ultrasonic surface waves," *Proceedings of the IEEE*, vol. 57, no. 6, pp. 1211–1213, 1969.

[23] A. Pohl, G. Ostermayer, and F. Seifert, "Wireless sensing using oscillator circuits locked to remote high-Q SAW resonators," *IEEE Transactions on Ultrasonics, Ferroelectrics, and Frequency Control*, vol. 45, no. 5, pp. 1161–1168, 1998.

[24] D. Dye, "The piezo-electric quartz resonator and its equivalent electrical circuit," *Proceedings of the Physical Society of London*, vol. 38, pp. 399–458, 1926.

[25] P. V. *et al*, "Theoretical and experimental analysis of high Q SAW resonator transient response in a wireless sensor interrogation application," *2012 IEEE International Frequency Control Symposium, IFCS 2012, Proceedings*, pp. 446–451, 2012.

[26] M. Takagi, S. Kanna, and E. Momosaki, "Surface acoustic wave device and method for designing same using resonators having different frequency-temperature characteristics," June 15 1999. US Patent 5 912 602.

[27] G. Martin, R. Kunze, B. Wall, and M. Weihnacht, "SAW resonators for temperature stable oscillators," *Proc. IEEE Ultrason. Symp.*, pp. 450–453, 2005.

[28] G. Martin, R. Kunze, and B. Wall, "Temperature-stable double SAW resonators," *IEEE Transactions on Ultrasonics, Ferroelectrics, and Frequency Control*, vol. 55, no. 1, pp. 199–207, 2008.

[29] N. Carvalho and *et al*, "Multisine signals for wireless system test and design," *IEEE Microwave Magazine*, vol. 9, no. 3, pp. 122–138, 2008.

[30] J. Hoagg, S. Lacy, V. Babuska, and D. Bernstein, "Sequential multisine excitation signals for system identification of large space structures," *American Control Conference, 2006*, no. iii, pp. 6 pp.–, 2006.

[31] A. Pohl and F. Seifert, "New applications of wirelessly interrogable passive SAW sensors," *IEEE Transactions on Microwave Theory and Techniques*, vol. 46, no. 12 PART 2, pp. 2208–2212, 1998.

[32] A. Oppenheim and R. Schafer, *"Digital Signal Processing"*. Prentice-Hall International Edition, 1975.

[33] M. Gasior and J. Gonzalez, "Improving fft frequency measurement resolution by parabolic and gaussian interpolation," *AB-Note-2004-021 BDI, CERN - AB Division*, Genevra Switzerland, February, 2004.

[34] S. Orfanidis, *"Introduction to Signal Processing"*. Prentice-Hall, Inc., 1995.

[35] R. P. Feynman, *"The Feynman Lectures on Physics, Vol.2"*. New Millennium Edition, 1963.

[36] V. Kalinin, "RF Rotary Couplers for Contactless Torque Sensors Based on SAW Resonators," *European Time and Frequency Forum, Toulouse*, 2008.

[37] J. W. Arthur, "Radio frequency coupler," May 22 1996. WO 96/37921.

[38] J. Beckley, V. Kalinin, M. Lee, and K. Voliansky, "Non-contact torque sensors based on SAW resonators," *Proceedings of the 2002 IEEE International Frequency Control Symposium and PDA Exhibition (Cat. No.02CH37234)*, pp. 202–213, 2002.

[39] SENSeOR, *Wireless SAW Strain gages measurement configurations.*

[40] "Shear modulus." `https://https://en.wikipedia.org/wiki/Shear_modulus`. Accessed: 2016-09-08.

[41] V. Kalinin, "Creep and hysteresis in saw strain sensors," *SAW Symposium*, Vienna Austria, 2014.

[42] V. Kalinin, "Modelling of hysteresis and creep in saw strain sensors," *Frequency Control Symposium (FCS), 2014 IEEE International*, pp. 0–3, 2014.